Mon. Not. R. Astron. Soc. **000**, 000–000 (0000) Printed 4 February 2008 (MN LATEX style file v2.2)

Probing the star formation history using the redshift evolution of luminosity functions

Saumyadip Samui⋆, Raghunathan Srianand†, Kandaswamy Subramanian‡
IUCAA, Post Bag 4, Ganeshkhind, Pune 411 007, India.

4 February 2008

ABSTRACT

We present a self-consistent, semi-analytical ΛCDM model of star formation and reionization. For the cosmological parameters favored by the WMAP data, our models consistently reproduce the electron scattering optical depth to reionization, redshift of reionization and the observed luminosity functions (LF) and hence the star formation rate (SFR) density at $3 \leq z \leq 6$ for a reasonable range of model parameters. While simple photoionization feedback produces the correct shape of LF at $z = 6$, for $z = 3$ we need additional feedback that suppresses star formation activities in halos with $10^{10} \lesssim (M/M_{\odot}) \lesssim 10^{11}$. Models with prolonged continuous star formation activities are preferred over those with short bursts as they are consistent with the existence of a Balmer break in considerable fraction of observed galaxies even at $z \sim 6$. The halo number density evolution from the standard ΛCDM structure formation model that fits LF up to $z = 6$ is consistent with the upper limits on $z \simeq 7$ LF and source counts at $8 \leq z \leq 12$ obtained from the Hubble Ultra Deep Field (HUDF) observations without requiring any dramatic change in the nature of star formation. However, to reproduce the observed LF at $6 \leq z \leq 10$, obtained from the near-IR observations around strong lensing clusters, we need a strong evolution in the initial mass function, reddening correction and the mode of star formation at $z \gtrsim 8$. We show that low mass molecular cooled halos, which may be important for reionizing the universe, are not detectable in the present deep field observations even if a considerable fraction of its baryonic mass goes through a star burst phase. However, their presence and contribution to reionization can be inferred indirectly from the redshift evolution of the luminosity function in the redshift range $6 \leq z \leq 12$. In our model calculations, the contribution of low mass halos to global SFR density prior to reionization reveals itself in the form of second peak at $z \geq 6$. However this peak will not be visible in the observed SFR density as a function of z as most of these galaxies have luminosity below the detection threshold of various ongoing deep field surveys. Accurately measuring the LF at high redshifts can be used to understand the nature of star formation in the dark ages and probe the history of reionization.

Key words: cosmology: early universe – theory – galaxies:formation – luminosity function – high-redshift – stars.

1 INTRODUCTION

Understanding how and when the dark ages ended and led to the reionization of the intergalactic medium (IGM) is one of the holy grails of modern cosmology. The collapse of the first non-linear structures and the associated star formation possibly provide the first sources of UV photons which ionized the IGM. Direct observations of these earliest star forming 'galaxies' is rapidly on the rise, with data constraining the luminosity functions of galaxies and hence the redshift evolution of star formation rate (SFR) density till $z \simeq 10$. At the same time tight constraints are being set on the epoch of reionization by studying spectra of the highest redshift QSOs and the ongoing WMAP satellite observations of the Cosmic Microwave Background (CMB) polarization. It is imperative to construct models of structure formation that explain the wealth of available data, and so probe the nature of star formation in the dark ages as well as in the post reionization era. This forms the basic motivation of the present work.

The absence of the Gunn-Peterson absorption (Gunn & Peterson, 1965) blue-ward of the Lyman-α emission from background QSOs had indicated that the IGM is highly ionized at least up to redshifts of about 5 or so. However, recent detections of a strong Gunn-Peterson trough in the spectra of QSOs with $z \simeq 6$ and limits obtained on the sizes of ionized regions around the highest z

⋆ E-mail: samui@iucaa.ernet.in
† E-mail: anand@iucaa.ernet.in
‡ E-mail: kandu@iucaa.ernet.in

QSOs, indicate a significantly neutral IGM above $z \sim 6$ (Wyithe et al. 2005; Fan et al. 2006). The CMB observations are still intriguing, with a recent downward revision of the the optical depth to electron scattering, from a $\tau_e = 0.17^{+0.08}_{-0.07}$ based on the first year WMAP data (Spergel et al. 2003), to a value $\tau_e = 0.09^{+0.03}_{-0.03}$ from the three year data (Spergel et al. 2006). The latter measurement would naively suggest a reionization redshift $7 \leq z_{re} \leq 12$. This is consistent with that indicated by the quasar observations. However, WMAP 3rd year data also indicate a lower power in density fluctuations (with $\sigma_8 = 0.74^{+0.05}_{-0.06}$) and also a redder power spectrum (with a scalar spectral index $n_s = 0.952^{+0.015}_{-0.019}$). Both these effects decrease the predicted number density of collapsed objects, and hence can make it potentially difficult to explain the observed $\tau_e \sim 0.09$ (Alvarez et al. 2006).

Direct measurements of luminosity function and hence the SFR density up to the redshift that is consistent with the z_{re} suggested by the WMAP data is now possible, thanks to the photometric dropout techniques (e.g. Steidel et al. 2003). For $z \lesssim 6$ we have several sets of observations from different groups which appear to be in reasonably good agreement with each other (Iwata et al. 2003; Sawicki & Thompson 2006; Bouwens & Illingworth 2006). These observations put tight constraints on luminosity functions at these epochs and hence on SFR density. However observational constraints on the luminosity function for redshifts $z > 6$ are scanty and have more uncertainty than the $z \lesssim 6$ data. Bouwens et al. (2005), based on the NICMOS-UDF data reported a rapid decline in the SFR density at $z \gtrsim 5$. In striking contrast, the SFR density estimated from Lyα emitters detected at $z = 5.7$ and 6.5 implies no substantial decrease with z (Hu & Cowie 2006). The decline in the SFR density is also not supported by near-IR observations of Richard et al. (2006) around lensing clusters, obtained with VLT/ISAAC. Selection biases and cosmic variance could provide possible reasons for the difference (Hu & Cowie 2006). As we will show here, clarifying this issue observationally is of paramount importance to probe the nature of the first star formation.

Reionization also feeds back on star formation by suppressing the collapse of the gas into low mass halos (Thoul & Weinberg 1996). It is then important to model the redshift evolution of luminosity function, SFR density and reionization simultaneously, in a self-consistent manner, taking account of such radiative feedback. We do this here adopting a semi-analytical approach. This is also motivated by the need to explore the sensitivity to model parameters in an extensive fashion.

In section 2 we outline our semi-analytic models for star formation and reionization and discuss how to compute the redshift evolution of the luminosity function and integrated source counts for high-z galaxies. The resulting reionization history is described in section 3, while sections 4 and 5 focus on the results for the UV luminosity function of high redshift galaxies. We elaborate further in section 6, the utility of the $z \geq 6$ luminosity functions in probing reionization history. The redshift evolution of the SFR density inferred from our models is presented in section 7, and a discussions of results and our conclusions are presented in the last section. In most of this work we use the cosmological parameters consistent with the recent WMAP data ($\Omega = 1$, $\Omega_m = 0.26$, $\Omega_\Lambda = 0.74$, $\Omega_b = 0.044$, $h = 0.71$, $\sigma_8 = 0.75$ and $n_s = 0.95$).

2 SEMI-ANALYTIC MODELS

2.1 Redshift evolution of star formation

The formation and evolution of galaxies and the associated star formation histories have been studied extensively using both numerical simulations and semi-analytic models (Chiu & Ostriker 2000; Choudhury & Srianand 2002; Springel & Hernquist 2003; Nagamine et al. 2006). Here, we use the modified Press-Schechter (PS) formalism of Sasaki (1994) to study the redshift evolution of the SFR density (see also Chiu & Ostriker (2000); Choudhury & Srianand (2002)). In this formalism the number density of collapsed objects having mass in the range $(M, M + \mathrm{d}M)$, which are formed at the redshift interval $(z_c, z_c + \mathrm{d}z_c)$ and survive till redshift z is, (Sasaki 1994; Chiu & Ostriker 2000)

$$\begin{aligned} N(M, z, z_c)\,\mathrm{d}M\,\mathrm{d}z_c &= N_M(z_c)\left(\frac{\delta_c}{D(z_c)\sigma(M)}\right)^2 \frac{\dot{D}(z_c)}{D(z_c)} \\ &\times \frac{D(z_c)}{D(z)}\frac{\mathrm{d}z_c}{H(z_c)(1+z_c)}\,\mathrm{d}M. \end{aligned} \quad (1)$$

Here, the overdot represents time derivative, $N_M(z_c)\,\mathrm{d}M$ is the number of collapsed objects per unit comoving volume within a mass range $(M, M + \mathrm{d}M)$ at redshift z_c, known as the PS mass function (Press & Schechter 1974), and δ_c is the critical over density for collapse, usually taken to be equal to 1.686 for a matter dominated flat universe ($\Omega_m = 1$). This parameter is quite insensitive to cosmology and hence the same value can be used for all cosmological models (Eke, Cole & Frenk 1996). Further, $H(z)$ is the Hubble parameter, $D(z)$ the growth factor for linear perturbations and $\sigma(M)$ the rms mass fluctuation at a mass scale M. The ratio $D(z_c)/D(z)$ gives the probability that a halo which collapsed at z_c survives till z. Note that $N(M, z, z_c)$ is the formation rate of halos weighted by their survival probability, and integrating it over z_c from z to ∞ gives the PS mass function $N_M(z)$ at any redshift z: that is $N_M(z) = \int_z^\infty N(M, z, z_c)\,\mathrm{d}z_c$.

Next, we assume that the SFR at z of a halo of mass M that has collapsed at an earlier redshift z_c, is given by (Chiu & Ostriker 2000; Choudhury & Srianand 2002)

$$\begin{aligned} \dot{M}_{\rm SF}(M, z, z_c) &= f_* \left(\frac{\Omega_b}{\Omega_m} M\right) \frac{t(z) - t(z_c)}{\kappa^2\, t^2_{\rm dyn}(z_c)} \\ &\times \exp\left[-\frac{t(z) - t(z_c)}{\kappa\, t_{\rm dyn}(z_c)}\right]. \end{aligned} \quad (2)$$

Here, f_* is the fraction of total baryonic mass in a halo that will be converted to stars. The function $t(z)$ gives the age of the universe at redshift z; thus, $t(z) - t(z_c)$ is the age of the collapsed halo at z. $t_{\rm dyn}$ is the dynamical time-scale and given by (Chiu & Ostriker 2000; Barkana & Loeb 2001)

$$t_{\rm dyn}(z) = \sqrt{\frac{3\pi}{32 G \rho_{\rm vir}(z)}}. \quad (3)$$

Here,

$$\begin{aligned} \rho_{\rm vir}(z) &= \Delta_c(z)\rho_c(z) \\ \Delta_c(z) &= 18\pi^2 + 82d(z) - 39d^2(z) \\ d(z) &= \frac{\Omega_m(1+z)^3}{\Omega_m(1+z)^3 + \Omega_\Lambda} - 1 \\ \rho_c(z) &= \frac{3H^2(z)}{8\pi G}. \end{aligned}$$

The duration of star formation activity in a halo depends on the value of κ. For a given value of κ star formation occurs in a contin-

uous mode with a peak at $\kappa\ t_{\rm dyn}$ and decaying exponentially afterward. Note that $\kappa \rightarrow 0$ corresponds to the star formation occurring in a single burst.

We can then calculate the cosmic SFR per unit comoving volume at a redshift z using,

$$\dot{\rho}_{\rm SF}(z) = \int_{z}^{\infty} {\rm d}z_c \int_{M_{\rm low}}^{\infty} {\rm d}M' \dot{M}_{\rm SF}(M', z, z_c) \times N(M', z, z_c). \quad (4)$$

The lower mass cutoff ($M_{\rm low}$) at a given epoch is decided by the cooling efficiency of the gas and different feedback processes. In the absence of UV background radiation $M_{\rm low}$ is decided only by the cooling efficiency of the gas. In the early universe, recombination line cooling from hydrogen and helium lines are favored as the heavier elements are absent. However, such cooling is effective only above temperatures of about 10^4 K. Thus gas in halos with virial temperatures in excess off 10^4 K can cool and collapse to form stars. However, if one can increase the H_2 content of the gas then molecular line cooling can lead to the formation of cold gas condensations within the low mass halos (Tegmark et al. 1997). Haiman, Abel & Rees (2000) have shown that such cooling can be efficient for $T_{\rm vir} \geq 300$ K. The presence of Lyman and Werner band photons that are produced by luminous objects can easily destroy these H_2 molecules. So survival of star formation activities in low mass halos is always very uncertain. In what follows we consider models with $M_{\rm low}$ corresponding to a virial temperature, $T_{\rm vir} = 10^4$ K (hereafter "atomic cooling model") and 300 K ("molecular cooling model").

Ionization of the IGM by UV photons enhances the temperature of the gas thereby increasing the Jean's mass for the collapse. Thus, $M_{\rm low}$ is increased in the ionized regions due to photoionization heating. It is known from simulations that the photoionizing background suppresses galaxy formation within halos with circular velocities (v_c) less than about 35 km s^{-1}, while the mass of cooled baryons is reduced by 50% for halos with circular velocities $\sim$ 50 km s^{-1} (Thoul & Weinberg 1996). However, the exact value will depend on the intensity and spectral shape of the ionizing background radiation. Therefore, the cutoff in v_c can in principle be redshift dependent (Benson et al. 2002; Dijkstra et al. 2004). In the ionized fraction of the universe, our models assume complete suppression of star formation in halos below circular velocity $v_c = 35$ km s^{-1} and no suppression above circular velocity of 95 km s^{-1}. For intermediate masses, we adopt a linear fit from 1 to 0 for the suppression factor (as in Bromm & Loeb, 2002). The ionized fraction of the universe itself, at a given epoch, is computed using the simple model of reionization described below.

Semi-analytical ΛCDM models of galaxy formation without feedback usually also overproduce the number of high luminosity galaxies compared to the observations (see Somerville & Primack, 1999). Further, recent observations of high-z galaxies suggest that the SFR in massive galaxies was higher at high-z (i.e. $z \simeq 2$) compared to that in the local universe, contrary to the naive predictions of hierarchical structure formation (Cowie et al. 1996; Juneau et al. 2005; Croton et al 2006). Thus, we need to incorporate the declining star formation activities in the massive halos. This can arise, physically, due to the effect of AGN feedback (Bower et al. 2005; Best et al. 2006). For simplicity we model this by multiplying the integrand in Eq. (4) with a suppression factor

$$f_{\rm sup} = \frac{1}{1 + \left(\frac{M}{10^{12} M_\odot}\right)^3} \quad (5)$$

which sharply decreases star formation in high mass halos above $10^{12} M_\odot$. The main conclusions of our work are insensitive to the exact nature of this cutoff as long as the typical mass above which star formation is suppressed is not much smaller than $10^{12} M_\odot$.

2.2 Redshift evolution of the luminosity function

Although many works emphasize the measurements of SFR density at different redshifts, the more directly observed quantity is rather the luminosity function. The SFR density is merely a conversion from the measured luminosity function to the star formation rate assuming a continuous star formation with some initial mass function (IMF) for the formed stars. So a more accurate comparison of theory with observations will be possible if we compare the luminosity function at different epochs computed from our semi-analytical models with the observed luminosity functions. Furthermore, very low mass halos could contribute significantly to the theoretically computed SFR density, but not at all to the detected individual galaxies (and hence the observed luminosity function or the inferred SFR density). Therefore it is important to calculate the luminosity functions predicted by our semi-analytic models to constrain parameters of our models more accurately.

The luminosity function is computed as follows. From "Starburst99" code [1] (Leitherer et al. 1999) we obtain $l_{1500}(t)$, the luminosity at 1500 Å as a function of time, produced for every solar mass being converted to stars in a single (instantaneous) starburst. This quantity depends mainly on the IMF and metallicity of the gas. In our model, star formation is a continuous process lasting for a few dynamical time. We therefore compute the luminosity of a galaxy of age T using

$$L_{1500}(M, T) = \int_{T}^{0} \dot{M}_{\rm SF}(M, T - \tau)\, l_{1500}(\tau)\, {\rm d}\tau. \quad (6)$$

Here, the age of the galaxy formed at z_c and observed at z is $T(z, z_c) = t(z) - t(z_c)$. As a check on our prescription for calculating the luminosity as function of time, we reconstruct the luminosity evolution of a galaxy undergoing a constant star formation using convolution integral in Eq. (6) and compare it with the luminosity evolution directly obtained from "Starburst99" code. This comparison, shown in Fig. 1 as an insert, demonstrates that our prescription could provide a fairly accurate representation of the luminosity expected from models with continuously varying SFR. In Fig 1 we show the luminosity at 1500 Å calculated with our prescription, from a galaxy with a variable SFR. The galaxy is assumed to collapse at $z_c = 10$ and form $10^6\ M_\odot$ of stars with a Salpeter IMF (and masses between $1 - 100\ M_\odot$), at a rate given by Eq. (2), and with $\kappa = 1,\ 1/10$ and $1/100$. As per our expectation, when κ becomes small (say $\kappa = 1/100$) the luminosity at 1500 Å as a function of time is close to that expected from a single star burst. It is also evident from Fig. 1 that the peak luminosity is higher and occurs earlier for lower values of κ.

Hence, for any given halo of mass M which collapses at z_c, and undergoes star formation as given by Eq. (2), one can compute its luminosity evolution. The luminosity can be converted to a standard absolute magnitude, say the AB magnitude using

$$M_{AB} = -2.5 \log_{10}(L_{\nu 0}) + 51.60 \quad (7)$$

[1] http://www.stsci.edu/science/starburst99

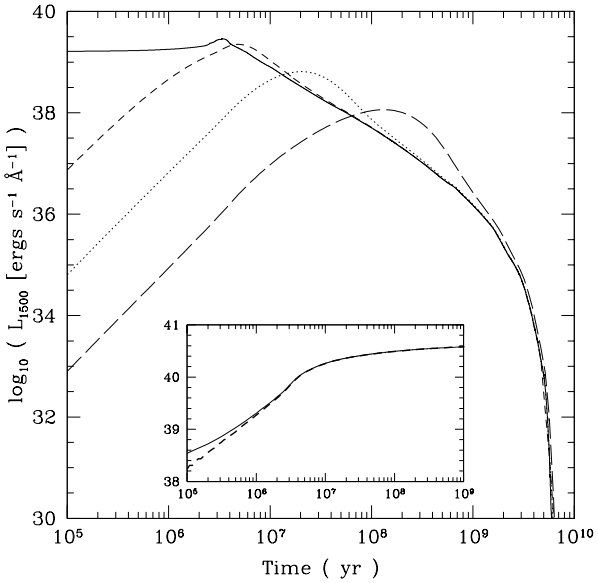

Figure 1. Luminosity at 1500 Å of a halo with stellar mass $10^6\ M_\odot$ collapsed at $z_c = 10$. The IMF is Salpeter from $1 - 100\ M_\odot$ with metallicity $Z = 0.0004$. The solid curve is for burst model (obtain from "Starburst99"). Other three curves are obtained by using Eq. (6) and the SFR given by Eq. (2) for $\kappa = 1$ (long-dashed), $1/10$ (dotted) and $1/100$ (short-dashed). In insert, we show the luminosity of a galaxy undergoing a continuous star formation at a rate of $1\ M_\odot\ \mathrm{yr}^{-1}$ for comparison. The solid curve is the result from "Starburst99" code (Fig. 54 of original 1999 dataset) and dashed curve is our model prediction. The IMF is Salpeter in the mass range $1 - 100\ M_\odot$ and the metallicity is $Z = 0.001$.

where the luminosity is in units of erg s^{-1} Hz^{-1} (Oke & Gunn 1983). The luminosity function $\Phi(M_{AB}, z)$ at any redshift z is then given by

$$\Phi(M_{AB}, z)\, \mathrm{d}M_{AB} = \int_z^\infty \mathrm{d}z_c\ N(M, z, z_c) \quad \frac{\mathrm{d}M}{\mathrm{d}L_{1500}}\ \frac{\mathrm{d}L_{1500}}{\mathrm{d}M_{AB}}\ \mathrm{d}M_{AB} \quad (8)$$

where $N(M, z, z_c)$ is given by Eq. (1). In what follows, we will be comparing the high redshift luminosity functions computed using Eq. (8) with observations. Further, one can directly integrate the theoretically computed luminosity function at a given z to a given luminosity limit, fold in a conversion factor between the luminosity and the SFR to obtain the SFR density at that redshift. Note even though Eq. (2) directly gives the SFR density, it is better to obtain it by integrating the luminosity function. This is because the SFR density is usually measured by integrating the observed luminosity function above some luminosity threshold (for example $0.3L^*_{z=3}$). This issue is dealt with in greater detail in section 7.

2.3 Integrated source counts

For redshifts $z \gtrsim 8$, Bouwens et al. (2005) give upper limits on the number of sources detected up to the limiting apparent magnitude that their observations reach for $8 < z < 12$. They have then used these upper limits to set limits on the the SFR density at $z \gtrsim 8$. In order to compare with such observation at high redshifts we also compute the integrated source counts as a function of the limiting apparent magnitude. The number of galaxies per unit solid angle in the sky per unit redshift interval with apparent magnitude less than a limiting magnitude m_0 is given by (Peebles 1993; Padmanabhan 2002)

$$\frac{\mathrm{d}n(z, m < m_0)}{\mathrm{d}\Omega \mathrm{d}z} = \mathcal{N}(z, m < m_0) r^2_{\mathrm{em}}(z) d_H(z) \quad (9)$$

where

$$d_H(z) = \frac{c}{H_0 \left[\Omega_\lambda + \Omega_m (1+z)^3\right]^{1/2}}$$

is the 'Hubble Radius' and

$$r_{\mathrm{em}}(z) = c \int_0^z \frac{\mathrm{d}z}{H_0 \left[\Omega_\lambda + \Omega_m (1+z)^3\right]^{1/2}}.$$

Further, $\mathcal{N}(z, m < m_0)$ is the comoving number density of object at redshift z having apparent magnitude less than m_0, i.e.

$$\mathcal{N}(z, m < m_0) = \int_{-\infty}^{M_0(z, m_0)} \Phi_{M_{AB}}(M_{AB}, z)\, \mathrm{d}M_{AB} \quad (10)$$

The relation between apparent magnitude and absolute magnitude is given by (Peebles 1993; Padmanabhan 2002)

$$m - M = 25 + 5 \log_{10}[3000(1+z) r_{\mathrm{em}}(z) H_0/c] - 5 \log_{10}\ h. \quad (11)$$

To give a rough idea of the numbers involved, suppose a $10^{10} M_\odot$ dark matter halo collapses at $z_c = 10$ and undergoes a burst of star formation, with a fraction $f_* = 0.5$ going into stars having a Salpeter IMF from $1 - 100\ M_\odot$. Let us assume that the metallicity of the gas is $Z = 0.0004$. Then the luminosity at early epochs (up to a few Myrs) is $\sim 1.4 \times 10^{42}$ ergs s^{-1} $\mathrm{Å}^{-1}$, corresponding to an absolute AB magnitude of -23.46 (with no extinction correction) or -21.82 (with an extinction correction factor of 4.5). The corresponding apparent magnitudes are 26.7 and 28.34 respectively. In the survey by Bouwens et al. the limiting magnitude was ~ 28.5. So the detection of these halos with present technology depends on the amount of dust reddening in these galaxies. If the galaxy under goes a continuous star formation then its luminosity can be much smaller, making it more difficult to detect.

Table 1. Values of n_γ for different model parameters[1].

$m_{\mathrm{low}}(M_\odot)$	$m_{\mathrm{up}}(M_\odot)$	Metallicity(Z)	n_γ
1	100	0.040	4800
1	100	0.020†	5675
1	100	0.008	6530
1	100	0.004	7245
1	100	0.001	8710
1	100	0.0004	10450
0.5	100	0.0004	7780
0.1	100	0.0004	4100
10	100	0.0004	33810
50	500	10^{-7}	83000‡

[1] All the models use Salpeter IMF with $\alpha = 2.35$.
† Solar metallicity ($Z_\odot$).
‡ Taken from Schaerer (2003).

2.4 Cosmological reionization

In order to calculate the radiative feedback at different redshifts we need to know the ionization history of the universe. For this pur-

pose, we consider the following simple model of reionization that assumes (i) all the baryons in the IGM are in the form of hydrogen and (ii) all the Lyman continuum photons that escape a star forming galaxy are used for reionizing the IGM. The fraction of ionized hydrogen (f_{HII}) evolves as (Barkana & Loeb 2001),

$$\frac{\mathrm{d}f_{HII}}{\mathrm{d}z} = \frac{\dot{N}_\gamma}{n_H(z)}\frac{\mathrm{d}t}{\mathrm{d}z} - \alpha_B n_H(z) f_{HII} C \frac{\mathrm{d}t}{\mathrm{d}z}. \quad (12)$$

Here, $\dot{N}_\gamma$ is the rate of UV photons escaping into the IGM and $n_H(z)$ is the proper number density of the hydrogen atoms. The clumping factor of the IGM, C, is defined as $C \equiv \langle n_H^2 \rangle / \bar{n}_H^2$ and α_B is the case B recombination coefficient, at $T = 3 \times 10^4$ K. The first term on the right is the rate of ionization and second term is rate of recombination, weighted by the f_{HII}, as recombinations take place only in the ionized region. $\dot{N}_\gamma$ is obtained from the SFR density using,

$$\dot{N}_\gamma = \frac{\dot{\rho}_{\rm SF}(z)(1+z)^3}{m_p} n_\gamma f_{esc}. \quad (13)$$

Here n_γ is the number of ionizing photons released per baryon of stars formed and f_{esc} is the fraction of these photons which escape from the star forming halo. The value of n_γ depends on the IMF of the forming stars. For a Salpeter IMF (with $m_{\rm low} = 0.1\ M_\odot$, $m_{\rm up} = 100\ M_\odot$) $n_\gamma \sim 4000$. However, for first generation of metal free stars, the IMF could be biased towards very massive stars. This can give much larger values for $n_\gamma \sim 80000$ (Schaerer 2003; Haiman & Bryan 2006). In Table 1 we summarize the values of n_γ for different IMFs and metallicities obtained from 'Starburst99' that are used in our subsequent calculations.

Clearly f_{HII} as a function of z depends on our choice of n_γ, f_{esc} and C. In what follows, we use $f_{esc} = 0.1$ and n_γ corresponding to the assumed IMF. For the clumping factor C, we have assumed the following simple form given by (Haiman & Bryan 2006)

$$C(z) = 1 + 9\left(\frac{7}{1+z}\right)^2 \quad (14)$$

for $z \geq 6$ and $C = 10$ for $z < 6$. We also compute the electron scattering optical depth (τ_e) in order to compare it with the recent WMAP observation.

Having established the basic framework of semi-analytic models, in the following sections we present our self-consistent results of reionization, luminosity function and SFR density.

3 REIONIZATION HISTORY IN DIFFERENT MODELS

The epoch of reionization and hence the electron scattering optical depth, τ_e, are sensitive to cosmological parameters, mode of star formation and escape fraction of UV photons, f_{esc}. We define z_{re} as the redshift when the ionized fraction f_{HII} becomes unity. In Table 2 we show z_{re} and τ_e for a range of parameters considered in our study keeping $f_{esc} = 0.1$, $f_* = 0.5$ and taking account of only the atomic cooled halos. Note $f_* = 0.5$ used here is constrained by the observed luminosity functions discussed in the following section. The recent WMAP data gives $\tau_e = 0.09 \pm 0.03$. Models which assume Salpeter IMF with $m_{\rm low} \leq 1\ M_\odot$, $\kappa = 1$ and a range of metallicities produce τ_e in the lower end of the allowed range from the WMAP 3rd year data. However, models considering star formation with a top-heavy IMF and adopting a lower value of κ produce slightly higher values of τ_e.

Table 2. Results of reionization for atomic cooling models:†

$m_{\rm low}\ (M_\odot)$	Z	σ_8	n_s	κ	z_{re}	τ_e
0.1	0.0004	0.75	0.95	1.00	5.9	0.066
0.5	0.0004	0.75	0.95	1.00	6.6	0.076
1	0.0004	0.75	0.95	1.00	7.0	0.080[a]
10	0.0004	0.75	0.95	1.00	8.4	0.097[f]
1	0.001	0.75	0.95	1.00	6.8	0.077
1	0.004	0.75	0.95	1.00	6.7	0.075
1	0.008	0.75	0.95	1.00	6.4	0.073
1	0.020	0.75	0.95	1.00	6.3	0.071
1	0.040	0.75	0.95	1.00	6.0	0.069[b]
1	0.0004	0.85	0.95	1.00	8.5	0.100
1	0.0004	0.95	0.95	1.00	9.7	0.122
1	0.0004	0.75	1.00	1.00	7.8	0.093
1	0.0004	0.85	1.00	1.00	9.3	0.117
1	0.0004	0.95	1.00	1.00	10.9	0.142[c]
1	0.0004	0.75	0.95	0.50	7.2	0.088
1	0.0004	0.75	0.95	0.33	7.0	0.091
1	0.0004	0.75	0.95	0.25	7.1	0.092
1	0.0004	0.75	0.95	0.20	7.0	0.093
1	0.0004	0.75	0.95	0.11	7.0	0.095[d]
10	0.0004	0.75	0.95	0.50	8.8	0.105
10	0.0004	0.75	0.95	0.25	8.3	0.111
10	0.0004	0.75	0.95	0.11	8.4	0.114[e]

†All the models assume $m_{\rm up} = 100\ M_\odot$, $f_* = 0.5$ and $f_{esc} = 0.1$.
[a]model A; [b]model B; [c]model C; [d]model D; [e]model E; [f]model F.

Therefore, atomic cooling models with cosmological parameters constrained by the 3rd year WMAP data ($\sigma_8 = 0.75$ and $n_s = 0.95$) produce consistent values of τ_e for a range of star formation scenarios. Also the inferred reionization redshifts are consistent with observations of the highest redshift QSOs (Fan et al. 2006) and Lyman-α emitters (Iye et al. 2006). Reionization histories for some of these models are shown in top panel in Fig. 2. From Table 2 it is also clear that the models with higher values of $m_{\rm low}$, σ_8 and n_s produce reionization at slightly higher redshifts with higher τ_e. Further, for a given value of $f_* f_{esc}$ the redshift of reionization only depends weakly on κ as integrated star formation and hence the total number of UV photons escaping a halo remains the same. However, τ_e is larger for smaller κ as most of the star formation in halos occur over a shorter time-scale (see Fig. 1) thereby establishing H II regions very quickly.

Now consider the effect of star formation in molecular cooled halos. Molecular cooled halos were proposed as a main source for early reionization in order to reproduce the high optical depth reported from the 1st year WMAP data. In Table 3 we have shown the results when star formation is also allowed in such halos. Reionization histories for some of these models are shown in bottom panel in Fig. 2. It can be noted that if we use $f_* = 0.5$ and $f_{esc} = 0.1$ also in the case of molecular cooled halos (model M_1) the resulting optical depth is higher than the value obtained from the WMAP 3rd year data. It is obvious from the table that inclusion of star formation in molecular cooled halos increases the value of τ_e. However, this need not always leads to a higher value of z_{re}. This happens because we self-consistently calculate the reionization history where the radiative feedback suppresses the star formation in smaller mass halos. Such an effect is very clear for model M_2. Without star formation in molecular cooling halos we had $z_{re} = 7.0$ and

Table 3. Results of reionization for molecular cooling models.[1,2,3]

$m_{low}(M_\odot)$	$m_{up}(M_\odot)$	n_γ	f_*	κ	z_{re}	τ_e
1	100	10450	0.50	1	10.8	0.145[a]
1	100	10450	0.10	1	5.9	0.105[b]
50	500	83000	0.50	1	14.2	0.194
50	500	83000	0.10	1	11.6	0.155[c]
10	100	33800	0.50	1	12.6	0.171
10	100	33800	0.10	1	10.0	0.134
1	100	10450	0.50	1/2	6.3	0.154
1	100	10450	0.50	1/4	6.4	0.162
1	100	10450	0.10	1/2	6.2	0.114
1	100	10450	0.10	1/4	6.2	0.121[d]
10	100	33800	0.10	1/2	6.4	0.143
10	100	33800	0.10	1/4	6.5	0.150
50	500	83000	0.10	1/2	7.8	0.166
50	500	83000	0.10	1/4	6.9	0.174

[1] All models assume $f_{esc} = 0.1$, $\sigma_8 = 0.75$ and $n_s = 0.95$.
[2] Atomic cooled halos have parameters similar to model A in Table 2.
[3] κ as given in the table is used for all the halos.
[a] model M_1; [b] model M_2; [c] model M_3; [d] model M_4.

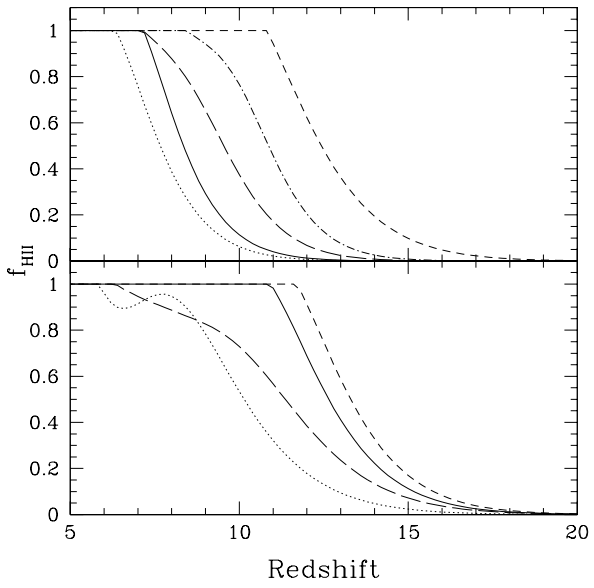

Figure 2. The reionization history for some atomic cooling (top panel) and molecular cooling (bottom panel) models. *Top panel:* The solid, dotted, short-dashed, long-dashed and dot-dashed curves are for models A, B, C, D and E respectively (see Table 2). *Bottom panel:* The solid, dotted, short-dashed and long-dashed curves are for models M_1, M_2, M_3 and M_4 respectively (see Table 3).

$\tau_e = 0.080$ (see model A in Table 2). Inclusion of star formation in molecular cooled halos has increased the value of τ_e to 0.105 but decreased z_{re} to 5.9.

From Table 3 one can conclude that to obtain τ_e within the 1σ value predicted by WMAP 3yr data star formation in molecular cooled halos should be in a continuous mode with normal Salpeter IMF if we consider the same efficiency factors as atomic cooled halos (i.e. $f_* = 0.5$ and $f_{esc} = 0.1$). The models with top-heavy IMF will produce consistent reionization only when we reduce either of these two efficiencies drastically. For example, a Pop III mode of star formation in molecular cooled halos, with $n_\gamma \sim 83,000$ leads to a $\tau_e \sim 0.17$ for $f_* f_{esc} = 0.01$, and so exceeds the τ_e inferred from the WMAP 3rd year data at a 2σ level. Clearly based on the constraints on reionization from WMAP data alone it is not possible to independently constrain both f_* as well as f_{esc}. We can only constrain the product $f_* f_{esc}$, and from Table 3, it appears that one needs this product to be at least smaller than ~ 0.01 for a top-heavy IMF. Thus the recent WMAP observations are better consistent with a low efficiency of the molecular cooled halos in reionizing the universe. This is in consonance with the results of Choudhury & Ferrara (2006), Haiman & Bryan (2006) and Greif & Bromm (2006).

We now have a set of models that can produce a τ_e consistent with the 3rd year WMAP data. However, as we will show in the next section, the luminosity functions and hence the global star formation rate density in these models can be very different. Therefore, one can use the observed luminosity functions at different epochs to get better constraints on our model parameters. We do this in what follows.

4 UV LUMINOSITY FUNCTION OF HIGH REDSHIFT GALAXIES

The luminosity function and SFR density as a function of z in our models will depend on the parameters associated with star formation, reionization in addition to the standard cosmological parameters. The parameters related to star formation like the IMF, metallicity and f_* could depend on redshift. Since the exact evolution of most of these quantities are difficult to predict, we compute luminosity function at a given z for a range of these parameters.

4.1 Observed luminosity functions

The observationally determined luminosity functions are taken from Sawicki et al. (2006) for $z = 3$ and $z = 4$, Iwata et al. (2003; 2007) for $z = 5$ and Bouwens & Illingworth (2006) for $z = 6$. Our model luminosity function is computed using luminosity at $\lambda = 1500$ Å. We obtain the observed luminosity function at $\lambda = 1500$ Å assuming flat spectrum in f_ν. For $z > 6$ we have constraints from three sets of observations. One is the upper limit based on the tentative detection of three candidate galaxies at $8 < z < 12$ by Bouwens et al. (2005) in the HUDF. The limiting magnitude of the Bouwens et al. (2005) survey varies from field to field, ranging from apparent magnitudes in the AB system of 27.2 to 28.7. The three candidate galaxies have H $\simeq 28$ and are detected in the two deep parallel fields observed with NICMOS covering a total area of 2.6 arc min^2 with 5σ limiting magnitudes of 28.5. The second observational constraint comes from the upper limits on the luminosity function at $z = 7$ derived by Mannucci et al. (2007) based on the absence of z'_{850} galaxies. The third study of relevance to high redshift star forming galaxies, is the deep near-IR imaging in the field of lensing clusters by Richard et al. (2006). In this study, Richard et al. (2006) derive the average luminosity function of galaxies at $6 \lesssim z \lesssim 10$.

4.2 Modeling the luminosity functions at $3 \leq z \leq 6$

In this section, we present theoretically computed luminosity functions at $3 \leq z \leq 6$. These are calculated using the formalism described in section 2. As reionization occurs at $z_{re} > 6$ the luminosity functions in this redshift range are not sensitive to the

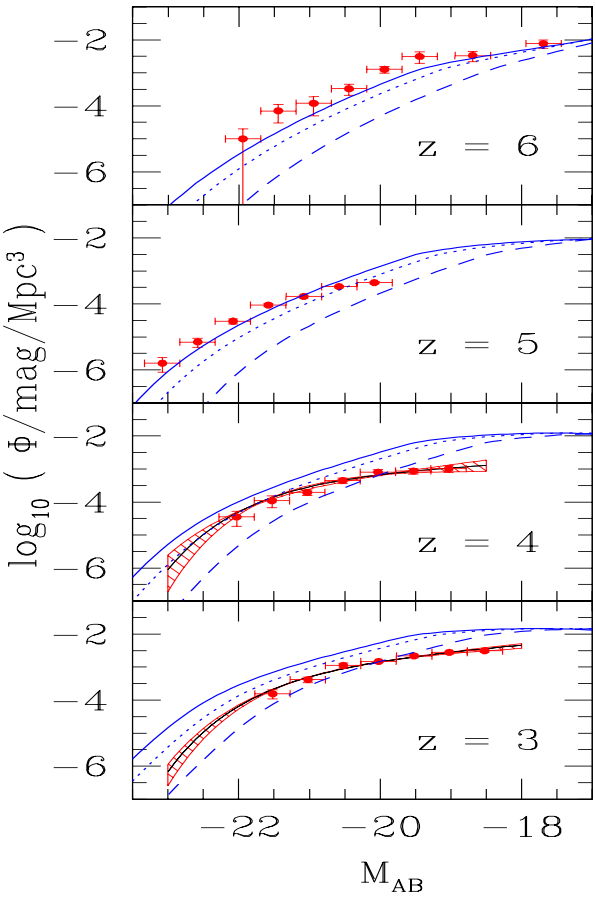

Figure 3. Luminosity function at different redshift bins. The solid, dotted and dashed curves are the predictions of models with lower mass cutoffs 1, 0.5 and 0.1 $M_\odot$ respectively. All the models assume Salpeter IMF with upper mass cutoff 100 $M_\odot$, metallicity $Z = 0.0004$, $\kappa = 1.0$ and $f_* = 0.5$.

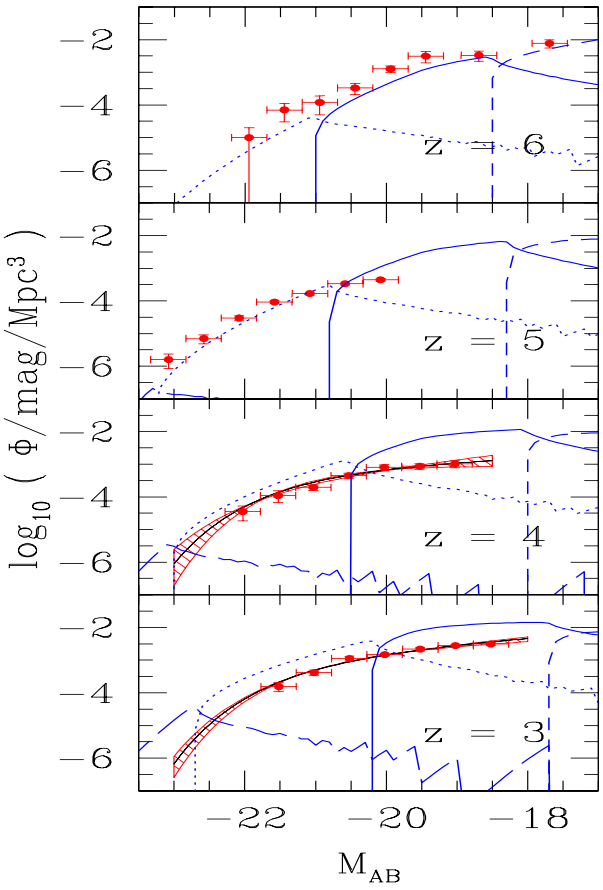

Figure 4. Contribution of halos with different mass ranges to the luminosity function. Curves are shown for mass range $10^9 - 10^{10}$ $M_\odot$ (short-dashed), $10^{10} - 10^{11}$ $M_\odot$ (solid), $10^{11} - 10^{12}$ $M_\odot$ (dotted) and $> 10^{12}$ $M_\odot$ (long-dashed). The model presented here assumes Salpeter IMF with lower mass cutoff 1 $M_\odot$ and upper mass cutoff 100 $M_\odot$, $Z = 0.0004$, $\kappa = 1.0$ and $f_* = 0.5$.

details of reionization history. In Fig. 3, we overplot our computed luminosity functions on the observed luminosity functions at different redshift bins. The curves are for a Salpeter IMF with an upper mass cutoff $m_{\rm up} = 100\ M_\odot$ and different lower mass cutoffs of $m_{\rm low} = 1,\ 0.5$ and $0.1\ M_\odot$, adopting a metallicity $Z = 4 \times 10^{-4}$ (i.e. $0.02\ Z_\odot$), $\kappa = 1$, and $f_* = 0.5$. We find that for the IMF considered above in a continuously star forming region the luminosity at 1500 Å depends very weakly on metallicity. For example changing Z from 10^{-7} to 4×10^{-3} produces a maximum change of 0.17 dex (Leitherer et al. 1999; Schaerer 2003). Thus we do not vary the metallicity in our models. The amount of reddening corrections we need to apply is an unknown quantity. In principle this can depend on the redshift. To start with we have applied an uniform reddening correction by a factor $\eta = 4.5$ (found by Reddy et al. (2006) at $z \simeq 2$) at all redshifts.

It is very encouraging to see our semi-analytic model with a simple prescription for continuous star formation reproduces the observed luminosity function reasonably well over the redshift range of interest here. Also as described before, these models have τ_e consistent with the WMAP 3rd year data (see Table 2). The flattening in the predicted luminosity function seen at the low luminosity end is due to the photoionization feedback we apply to the halos with $v_c \leq 90$ km s^{-1}. It is clear from the figure that the observed luminosity function at $z = 5$ and 6 are well reproduced by our models with $m_{\rm low} = 1\ M_\odot$. The models with $m_{\rm low} = 0.1\ M_\odot$ under predict the luminosity functions at the high luminosity end by more than an order of magnitude. Basically, lowering $m_{\rm low}$ from 1 to $0.1\ M_\odot$ makes the individual halos with a given star formation rate to appear ~ 1 mag fainter and moves the luminosity function along the x-axis towards the low luminosity (high AB mag) end. Thus in order to explain the observed luminosity function with $m_{\rm low} < 1\ M_\odot$, f_*/η has to be higher than $0.5/4.5$.

However, our model with $m_{\rm low} = 1\ M_\odot$ over produces the luminosity function by more than 0.4 dex at a given luminosity at $z = 3$ and 4 (Fig. 3). It is clear from the figure that our models can reproduce the brighter end ($M_{\rm AB} < -20$) of the luminosity function for $0.1 \leq m_{\rm low}(M_\odot) \leq 0.5$ at these redshifts. Thus it appears that a good agreement can be obtained by decreasing $m_{\rm low}$ with decreasing redshift keeping f_* and η constant. Such an evolution of $m_{\rm low}$ may naturally be obtained due to the increasing enrichment of the gas with the metals, by the previous generation of stars, as one goes to lower redshifts. At the same time, decreasing f_* (or increasing η) with decreasing redshift keeping the IMF constant will also provide similar fits.

Even though our models broadly reproduce the observed luminosity functions, it is obvious from Fig. 3 that they over-produce the number of objects at lower luminosities especially at lower red-

shifts. Note that the photoionization feedback we use affects star formation in halos with $v_c < 90$ km s^{-1}. This is marked by the break seen in our model luminosity functions at lower luminosity. Clearly this break occurs at absolute magnitudes $M_{\rm AB} > -19.5$ suggesting that some additional feedback may be needed to suppress star formation even in halos with v_c higher than 90 km s^{-1}. To know the range of mass where we still need more suppression of star formation we have plotted the contribution of different mass range to the luminosity function in Fig. 4. It is evident from this figure that one needs more suppression in halos with mass $10^{10} - 10^{11}\ M_\odot$. This will be the rough range even if we consider $m_{\rm low} = 0.1\ M_\odot$. In our models $10^{11}\ M_\odot$ corresponds to $v_c = 130$ and 145 km s^{-1} respectively for $z = 3$ and 4. Perhaps starburst driven galactic winds from these halos may provide such a negative feedback. Pettini et al. (2001) have reported large scale outflows from $z \sim 3$ Lyman break galaxies that have a typical dynamical mass of about $10^{10}\ M_\odot$. Recently, Croton et al. (2006) have noted that the expulsion of hot gas due to supernova feedback affects halos with v_c up to 200 km s^{-1} in their semi-analytic models implemented on the millennium dark matter simulations. Thus while radiative feedback alone gives the correct shape of the observed luminosity function for $z \geq 5$, we need additional feedback for halos $95 \lesssim v_c({\rm km\,s^{-1}}) \lesssim 150$ in order to explain the $z \sim 3$ luminosity functions. Further, it is clear from Fig. 4 that luminosity functions over the observed range, are insensitive to the exact nature of the high mass cutoff in Eq. (5), as long as the star formation is suppressed in massive halos with $M > 10^{12}\ M_\odot$.

There are other parameters in our model that will change the luminosity of a given halo. We explore the effect of these model parameters on the luminosity function below. For reference, we will take the model with $m_{\rm low} = 1\ M_\odot$, and $Z = 0.0004$ and other parameters as above as the fiducial model (called Model A). Note that the reionization history for this model is also denoted as model A in Table 2.

First, we study the sensitivity of our results to the mode of star formation. The burst mode of star formation corresponds to the limit $\kappa \to 0$. We show in Fig. 5, the luminosity function for various redshifts taking different values of $\kappa = 1/9, 1/5, 1/2, 1$. The solid curves in the figure are for our fiducial model A. For models with $\kappa < 1$, we suitably scale f_* to match the observed luminosity function. As one decreases κ and goes towards the burst mode of star formation, the number of objects in the brighter end of the luminosity function, significantly increases. However better matching to the data can be obtained by lowering the value of f_*. For example, at $z = 6$ models reproduced the observed luminosity function for $f_* = 0.32,\ 0.20$ and 0.13 for $\kappa = 1/2,\ 1/5$ and $1/9$ respectively. Similarly at $z = 3$ we need $f_* = 0.17,\ 0.10$ and 0.07 for $\kappa = 1/2,\ 1/5$ and $1/9$ respectively. However, in order to keep the z_{re} high enough we need to preserve $f_* f_{esc}$ by increasing f_{esc} whenever we decrease f_* from 0.5. Therefore, in the framework of models discussed here observations of luminosity function at $z \lesssim 6$ can be reproduced by both the continuous as well as burst mode of star formation. However, in both the cases we need to allow for redshift evolution of either of $m_{\rm low}$, η or f_*. Decrease in $m_{\rm low}$ and increase in η with decreasing redshift can naturally arise with the expected redshift evolution of metallicity.

The nature of the IMF and duration of the star formation activities in a given galaxy can be obtained by fitting the observed spectral energy distribution (SED) with synthetic spectrum. Eyles et al. (2007) have fitted the rest frame UV-optical SED of 30 galaxies at $z \sim 6$ with reliable photometric or spectroscopic redshifts. They found a surprisingly large fraction of galaxies with a signatures of substantial Balmer breaks indicating the presence of an underlying old stellar population that dominates the stellar masses. The calculated age of these objects are in the range 180-640 Myr and stellar masses in the range $1 - 3 \times 10^{10}\ M_\odot$. It is interesting to note that in our model A that fits the $z = 6$ luminosity function reasonably well, the observed range in the luminosity is produced by halos with stellar masses in range $3 \times 10^8 - 2 \times 10^{10}\ M_\odot$. The dynamical time-scale at this epoch is 124 Myr and thus the expected time-scales for the star formation activity in these models, are consistent with that noted by Eyles et al. (2007). When we consider an IMF with $m_{\rm low} = 1\ M_\odot$ the Balmer break naturally occurs in the spectrum. No break will be visible in the photometric data if one uses $m_{\rm low} = 10\ M_\odot$. Thus our models which fit the luminosity function will also be consistent with the SED of few of the galaxies observed by Eyles et al. (2007). When we consider $\kappa = 1$, we require roughly 50% of the baryon mass to go through star formation over few dynamical time-scale. This is again consistent with the median gas fraction of 50% and the corresponding stellar mass inferred from the high-z Lyman break galaxies (Erb et al. 2006).

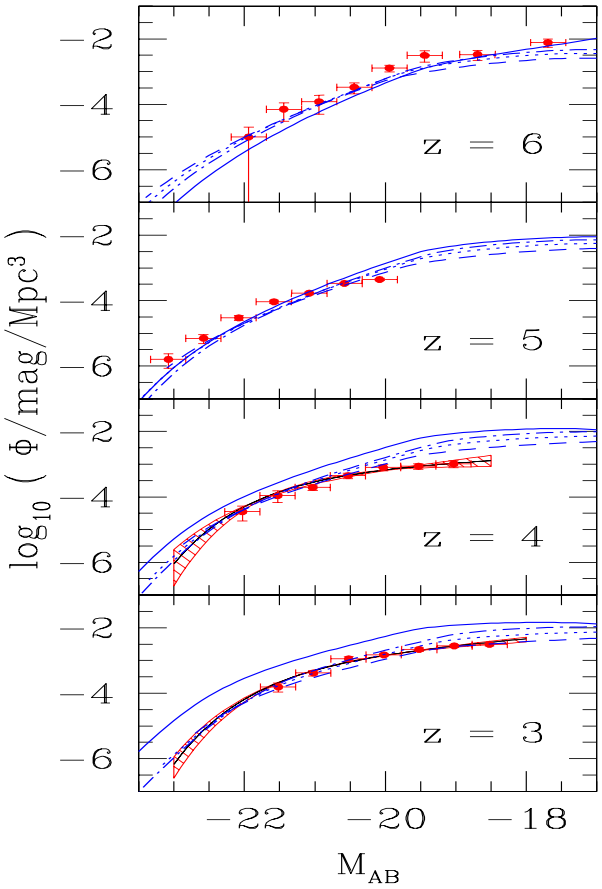

Figure 5. Effect of κ on the predicted luminosity function. Curves are shown for $\kappa = 1.0$ (solid), 0.50 (dot-dashed), 0.20 (dotted) and 0.11 (dashed). All of them are for Salpeter IMF with lower mass cutoff 1 $M_\odot$ and upper mass cutoff 100 $M_\odot$ and metallicity 0.0004. For $\kappa = 1.0$ we have assumed $f_* = 0.5$. For the lower values of κ we have used the lower values of f_* to match the observations.

Finally, in Fig. 6, we have considered the sensitivity of our results to changes in σ_8 and n_s, from the values favored by WMAP 3yr data. As expected an increase in σ_8 or n_s leads to larger number of objects at any given luminosity, at all redshifts. This basically

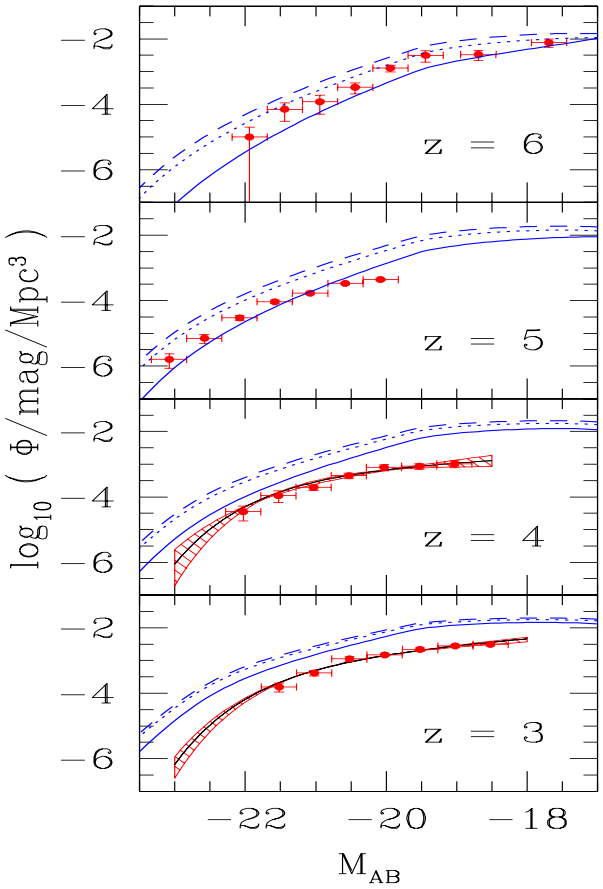

Figure 6. Dependence of luminosity functions on σ_8 and n_s. Solid curves are for $\sigma_8 = 0.75$ and $n_s = 0.95$ i.e. the WMAP 3rd yr cosmological parameters. The dotted lines are for $\sigma_8 = 0.85$ and $n_s = 0.95$. The dashed lines represent the WMAP first yr parameters i.e. $\sigma_8 = 0.85$ and $n_s = 1.00$. All of them are for Salpeter IMF with lower mass cutoff 1 $M_\odot$ and upper mass cutoff 100 $M_\odot$ and metallicity 0.0004. We have taken $\kappa = 1.0$ and $f_* = 0.5$.

reflects the fact that increasing σ_8 or n_s increases the number of collapsed halos. So the same data requires a lower value of f_*, for higher σ_8 or n_s.

We see therefore that combining a fairly simple model of star formation with the modified Press-Schechter formalism (according to the Sasaki prescription) one can fit the whole range of high redshift observed galaxy luminosity functions from $z = 3$ to $z = 6$, for a reasonable range of parameters. The feedback due to photoionization is sufficient to explain the $z = 6$ luminosity function. Whereas we need additional feedback, possibly due to galactic scale super winds driven by supernovae, to explain the low luminosity end for $z = 3$. We now proceed to our model predictions for the higher redshift range.

5 CONSTRAINING STAR FORMATION AT $z > 6$

In this section, we compare our model predictions with observations at $z > 6$. As one expects the epoch of reionization to fall in this redshift range (see Tables 2 and 3), our model predictions for a given z will be very sensitive to the reionization history. In addition one may need to consider the effects of molecular cooled halos

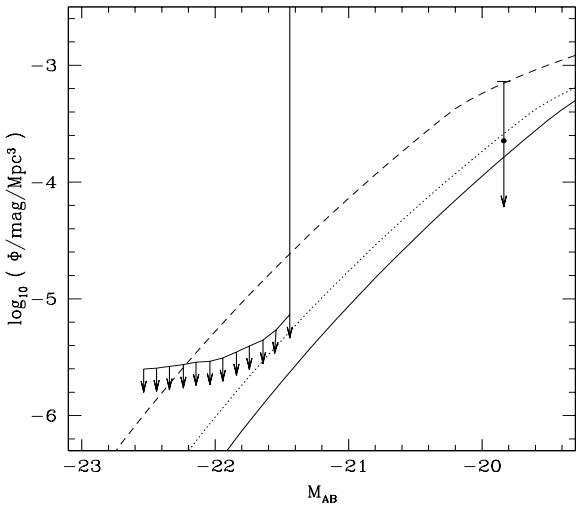

Figure 7. Luminosity function at $z = 7$. The observed data points are taken from Mannucci et al. (2007). The upper limit at $M_{AB} = 19.8$ is from Bouwens et al. (2004). The solid and dashed curves are for models A and F as in Table 2 respectively. The dotted line is for the models with $\kappa = 0.5$, f_* = 0.32 and rest of the parameters as in model A.

prior to reionization. At redshifts $z > 6$, in the absence of spectroscopic redshift measurements we have observational constraints in the form of integrated source counts and average luminosity functions obtained over a large redshift range. Here, we make predictions for both sets of observations, so as to probe the nature of star formation at such high redshifts.

5.1 UV Luminosity function

First we consider the upper limits on the luminosity function at $z = 7$ given by Mannucci et al. (2007). In Fig. 7 we show the observed luminosity function as well as the theoretically predicted luminosity functions at $z = 7$. The continuous curve is for model A and dotted curve in Fig. 7 is for model A with $f_* = 0.32$ and $\kappa = 0.5$. Both these models fit the $z = 6$ luminosity function well (see section 4). It is clear from the figure that the luminosity function predicted by these models are consistent with the null detection of galaxies by Mannucci et al. (2007). Note we have used $\eta = 4.5$ in our calculations. From the figure we can infer that a slightly lower value of η is also allowed by the observations. If we just follow the line of arguments we have presented in the last section, for $z \geq 6$ we expect the $m_{\rm low}$ to be higher than 1 $M_\odot$. The dashed line is for model F that has $m_{\rm low} = 10\ M_\odot$ and $\eta = 4.5$. Clearly this model over produce the number of high luminosity objects. The difference will become wider if we use a lower value of η. Thus, the upper limits in the luminosity function at $z = 7$ can be understood as due to just the effect of redshift evolution of dark matter halos from the standard structure formation, without a strong evolution in the nature of star formation. Labbe et al. (2006) using the Spitzer observations of candidate galaxies at $z \sim 7$ in UDF found that these galaxies have typical stellar mass of $1 - 10 \times 10^9\ M_\odot$ by fitting the SED. The typical age of these galaxies are $50 - 200$ Myr with average star formation rate of $25\ M_\odot\ {\rm yr}^{-1}$ assuming a constant star formation model. The age of these galaxies are then consistent with $\kappa \gtrsim 1/2$ in our model. This confirms that the detected candidates are undergoing prolonged star formation activities consistent with our model prediction.

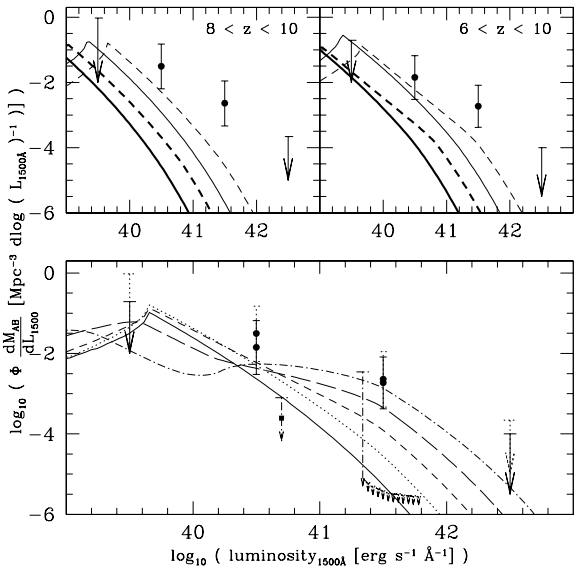

Figure 8. Luminosity function for $z = 9$ (top left panel) and $z = 8$ (top right panel). The solid and dashed lines corresponds to model A and model F respectively. The thick lines assume $\eta = 4.5$ while the thin lines are for $\eta = 1$. Bottom panel shows the redshift evolution of luminosity function for model F with $\eta = 1$. Curves are drawn for $z = 10$ (solid), 9 (dotted), 8 (short-dashed), 7 (long-dashed) and 6 (dash-dotted). The observed points for $6 < z < 10$ (range 2) and $8 < z < 10$ (range 1) are shown with errorbar in solid and dashed lines respectively. The Luminosity function at $z = 7$ from Mannucci et al. 2007 are given by dot-dashed lines.

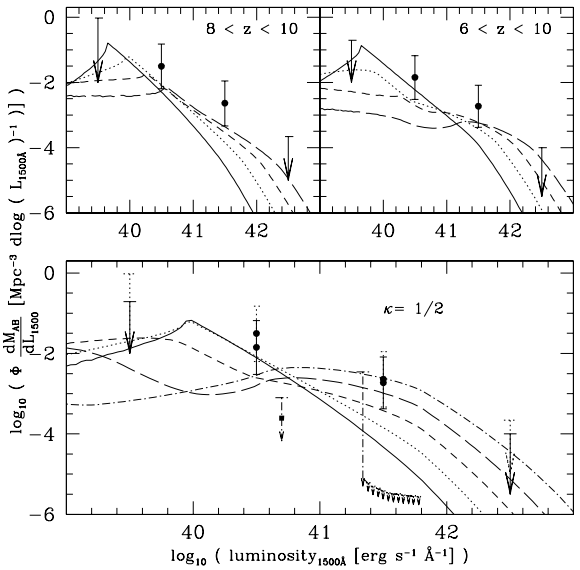

Figure 9. The variation of the luminosity functions for $z = 9$ (top left panel) and $z = 8$ (top right panel) with κ. All models assume the top heavy IMF, $\eta = 1$ and other parameters as in model A. The curves are for $\kappa = 1$ (solid), $\kappa = 1/2$ (dotted), $\kappa = 1/4$ (short-dashed) and $\kappa = 1/9$ (long-dashed). Bottom panel shows the redshift evolution of luminosity function for $\kappa = 1/2$. Curves are drawn for $z = 10$ (solid), 9 (dotted), 8 (short-dashed), 7 (long-dashed) and 6 (dash-dotted). The observed points for $6 < z < 10$ (range 2) and $8 < z < 10$ (range 1) are shown with errorbar in solid and dashed lines respectively. The Luminosity function at $z = 7$ from Mannucci et al. 2007 are given by dot-dashed lines.

The observational situation, however is not that simple as Richard et al. (2006) have reported the detection of a large number of $z \geq 6$ candidate galaxies in their search towards strong lensing clusters. In Fig. 8 we compare our model predictions with that obtained by Richard et al. (2006). It is important to note that spectroscopic redshifts are not available for the objects detected by Richard et al. (2006). Thus they have obtained only the average luminosity function either in the redshift range $8 < z < 10$ (called range 1) or $6 < z < 10$ (called range 2). Our model predictions are computed at the redshifts in middle of these ranges. In the top left and right panels in Fig. 8, we have shown our model predictions for $z = 9$ (for range 1) and $z = 8$ (for range 2) respectively. The thick solid and dashed line are respectively for model A and the top-heavy model F with $\eta = 4.5$. The corresponding thin lines are for $\eta = 1$. Clearly the luminosity functions derived from Richard et al.'s data can not be explained by simply changing $m_{\rm low}$ as we have done for $z \leq 7$. Even the model with no extinction correction and a top heavy IMF (i.e. $m_{\rm low} = 10\ M_{\odot}$) under predicts the abundance of the higher luminosity galaxies inferred by Richard et al. Our predictions for the luminosity function in range 2 is in slightly better agreement with the data when we use $\eta = 1$ than that for the range 1.

To investigate this issue further, in the bottom panel of Fig. 8 we show the redshift evolution of luminosity function for the model with no extinction correction ($\eta = 1$) and a top heavy IMF. The lines are for $z = 10$ (solid), 9 (dotted), 8 (short-dashed), 7 (long-dashed) and 6 (dash-dotted). The observed luminosity functions for range 1 and range 2 are shown with errorbar in dashed and solid lines respectively. Also the upper limits on the observed luminosity function at $z = 7$ are shown with arrows. The sharp cutoff seen in the low luminosity end of the luminosity function for $z \geq 8$ is due to the cooling cutoff at $T_{\rm vir} = 10^4$ K. The flattening in the luminosity function for $z \leq 7$ seen in the figure is due to radiative feedback, as reionization in this model occurs at $z_{re} = 8.4$ (see Table 2 for details). All our models clearly under produce the luminosity function at $8 < z < 10$. It is also clear from the figure that this model also over produces the abundance of $z = 7$ galaxies compared to that inferred by Mannucci et al. (2007) (See Fig. 8). Thus to fit the Richard et al.'s data one has to increase the luminosity of individual galaxies only at $z \geq 8$.

Next we investigate whether going over to a burst mode of star formation will yield a better match to Richard et al.'s data. In order to examine this possibility, we have shown in Fig. 9 our model predictions for the luminosity functions at $z = 9$ (right panel) and $z = 8$ (left panel) for a range of κ. The models also assume a top heavy IMF with a mass range $10 - 100\ M_{\odot}$, no extinction correction (i.e. $\eta = 1$) and all the other parameters as in model A. The curves are for $\kappa = 1$ (solid), $\kappa = 1/2$ (dotted), $\kappa = 1/4$ (short-dashed) and $\kappa = 1/9$ (long-dashed). We see that a moderate decrease in the value of κ by a factor of $2 - 4$ could make the model consistent with the Richard et al. data, especially if these galaxies are at $z \sim 8$ (also see bottom panel of Fig. 9 for the redshift evolution of the luminosity function for model with $\kappa = 1/2$). A decrease of κ to even smaller values, say to $\kappa = 1/9$ leads to a decrease in the number of lower luminosity galaxies, at $z = 8$, but matches the Richard et al. data if the detected galaxies had a redshift range $8 < z < 10$. Even this agreement is only with the lower end of the numbers allowed by the error bars given by Richard et al.

In Fig. 10 we plot the mass range contributing to different lu-

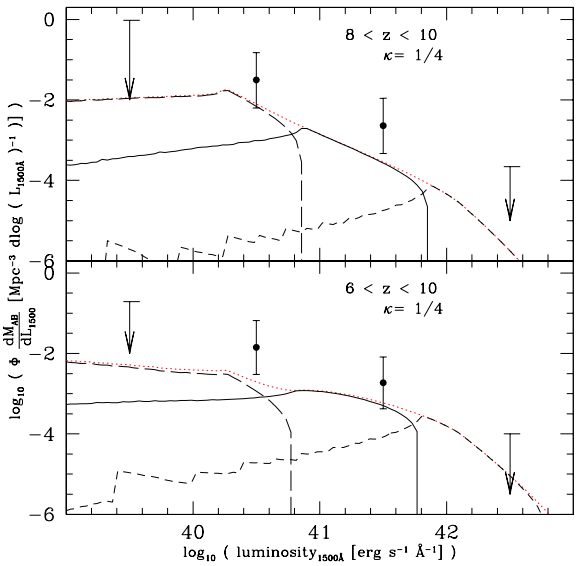

Figure 10. Contribution to the luminosity function by different mass range. Curves are drawn for a top-heavy IMF ($10 - 100\ M_\odot$), $\kappa = 1/4$ and $\eta = 1.0$ for $z = 9$ (top) and $z = 8$ (bottom). Long dashed lines are for contribution coming from halos with mass $M \leq 10^9\ M_\odot$, solid lines are for $10^9\ M_\odot \leq M \leq 10^{10}\ M_\odot$ and short dashed lines are for mass $M \geq 10^{10}\ M_\odot$. Dotted lines represent the total luminosity functions.

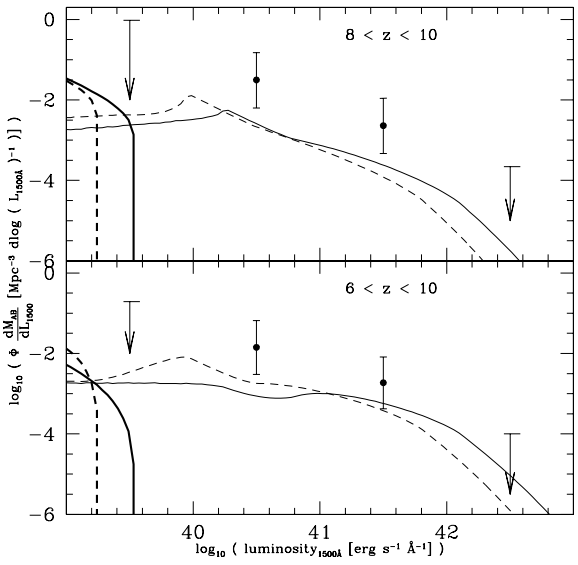

Figure 11. Luminosity function calculated for $z = 9$ and 10 when we add the contribution from the molecular cooled halos. We have assumed a top heavy IMF from 10 to 100 $M_\odot$ with $\eta = 1.0$. For atomic cooled halos $f_* = 0.50$ and for molecular cooled halos $f_* = 0.10$. We have shown the luminosity functions for $z = 9$ (top) and $z = 8$ (bottom) with $\kappa = 1/4$ (solid line) and $1/2$ (dashed line). The contribution coming from the molecular cooled halos are shown with thick lines where as thin lines represent the contribution from atomic cooled halos.

minosity ranges for $\kappa = 1/4$ for $z = 8$ and $z = 9$. The luminosity of galaxies that are detected by Richard et al.(2006) are produced by galaxies with dark matter mass of $\gtrsim 10^9\ M_\odot$, and for our models this corresponds to a stellar mass of $\gtrsim 10^8\ M_\odot$. This is roughly consistent with the stellar mass estimation of Richard et al. (2006). The objects with luminosity greater than 10^{42} erg s^{-1}Å^{-1} are produced by dark matter halos with $M \geq 10^{10}\ M_\odot$. Our model predictions are consistent with the absence of such very bright galaxies. Richard et al. (2006) obtained a SFR of individual galaxies in the range $10 - 40\ M_\odot$ yr^{-1} using template fitting method. In our case the SFR of the galaxy is a function of time typically lasting for 4κ times the dynamical time-scale. However, we can write the average SFR in a given halo as,

$$SFR = \left(\frac{10}{\kappa}\right)\left(\frac{M}{10^9 M_\odot}\right)\left(\frac{f_*}{0.5}\right)\left(\frac{1+z}{10}\right)^{3/2} M_\odot\ yr^{-1} \quad (15)$$

For $\kappa = 1/4$ the typical average SFR in the halos in our model is $40\ M_\odot$ yr^{-1}. This is consistent with the range found by Richard et al. (2006) (see their Tables C2 and C3).

In all the models discussed till now the effect of molecular cooled halos has not been considered. We expect star formation to be going on in some of the molecular cooled halos at least prior to the epoch of reionization and such a star formation is thought to be a very important component of contemporary models of reionization. Fig. 11 shows the expected range in luminosity from the molecular cooled halos with $f_* = 0.1$ (thick lines). We have drawn curves for top-heavy IMF (i.e. $10-100\ M_\odot$), $\eta = 1.0$ and $\kappa = 1/4$ (solid) and $1/2$ (dashed). Clearly the expected luminosity is below the detection limits achieved in the present day deep imaging surveys. Thus even if the molecular cooled halos are present in the early universe they will not contribute to the observed luminosity function (or for that matter to the inferred star formation rate density). However, star formation in molecular cooled halos provides additional Lyman continuum photons there by making reionization to occur earlier (see Table 3). This implies a relatively greater suppression of low mass halos due to reionization feedback, and in turn will lead to more and more difficulty in explaining the Richard et al. points. Note that while plotting Fig. 11 we have not considered the contribution of molecular cooled halos to the reionization in a self-consistent way. We will discuss the effect of reionization feedback on the predicted luminosity function in section 6.

5.2 Integrated source count at $8 \leq z \leq 12$

In Fig. 12, we show our model predictions of integrated source count at $8 < z < 12$ as a function of the limiting apparent magnitude for an area of 2.6 arcmin^2 (as in Bouwens et al. 2005). The redshift range covered is similar to the range 1 in Richards et al. (2006). The thick and thin solid lines show the predictions for model A with $\eta = 4.5$ and $\eta = 1$ respectively. The corresponding dashed lines are for $m_{\rm low} = 10\ M_\odot$. From Fig. 12, it is clear that the integrated source counts predicted by the continuous star formation models (with $m_{\rm low} \leq 10\ M_\odot$) will always be below the upper limit obtained by Bouwens et al. (2005) irrespective of f_* and η. However, if the 3 candidate galaxies tentatively identified in the Bouwens et al. (2005) data become confirmed as high-z galaxies, then our continuous star formation models will fail to reproduce their abundance.

We have also computed the source counts for the burst models discussed in Fig. 9. They are shown in Fig 13. The models with a top heavy IMF and with $\kappa > 1/2$ predicts number counts less than the upper limit given by Bouwens et al., while the model with $\kappa = 1/4$ gives counts slightly larger. However the model with $\kappa = 1/9$ over predicts the number counts and so is probably ruled out

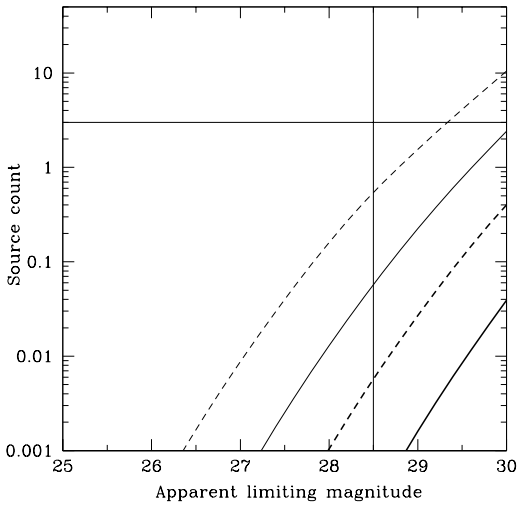

Figure 12. Integrated galaxy count as a function of apparent magnitude for the $8 < z < 12$ in an 2.6 arcmin^2 survey area. We have considered parameters as in model A, except for varying η and $m_{\rm low}$. The thick and thin solid lines show the source count predictions for model A with $\eta = 4.5$ and $\eta = 1$ respectively for $m_{\rm low} = 1 M_{\odot}$. The thick and thin dashed lines shows the corresponding source counts for a top heavy mass function with $m_{\rm low} = 10 M_{\odot}$, and all other parameters as in model A. The horizontal line corresponds to a detection of three galaxies in the above redshift range. The vertical line shows the 5σ limit of 28.5, for the Bouwens et al. detections.

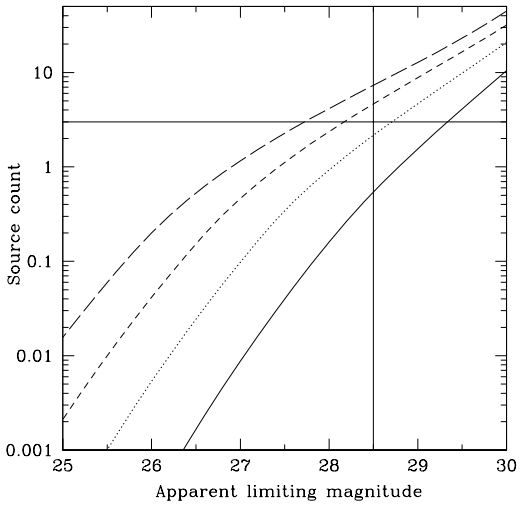

Figure 13. Total number of galaxy count as a function of apparent magnitude for the $8 < z < 12$ in an 2.6 arcmin^2 survey area, for the models of Fig. 9 (top panels). The line styles are are the same as in Fig. 9. The horizontal line corresponds to a detection of three galaxies in the above redshift range. The vertical line shows the 5σ limit of 28.5, for the Bouwens et al. detections.

by the Bouwens et al. data. It appears that having a top heavy IMF and a moderate decrease of κ can make our models consistent with both the Richard et al. and the Bouwens et al. data if one allows for 2σ errors. Note that one of the uncertain factors could be the effect of amplification bias in the estimation of luminosity function by Richard et al. (2006).

In summary, we have reproduced different sets of observations available in the literature for $z > 6$. The upper limits on the luminosity function for $z = 7$ obtained by Mannucci et al. (2007) and the upper limits on the integrated source counts for $8 \leq z \leq 12$ as a function of limiting apparent magnitudes by Bouwens et al. (2005) are consistent with the continuous star formation models that fits $z \leq 6$ luminosity function. The decline in the number density of sources at high redshifts can just be explained from the decline in the halo number density expected from structure formation models alone without any dramatic change in the nature of star formation activities at $z \geq 6$. In the language of observers these data at $z > 6$ are consistent with the pure number density evolution expected from the ΛCDM model without any luminosity evolution. However, these models fail to reproduce the luminosity function inferred by Richard et al. (2006) based on galaxies detected around strong lensing clusters. Such models will also fail if the three candidate galaxies identified by Bouwens et al. (2005) are confirmed as high-z galaxies. For the cosmological parameters constrained by WMAP 3rd year data both these observations can only be explained if star formation occurs in a burst mode (i.e. $\kappa < 1/2$) with high efficiency, top-heavy IMF and no reddening corrections for UV light. Thus if Richard et al. (2006) observations are correct then one needs a sudden change in the nature of the star formation at $z \geq 8$. In other words we need a strong luminosity evolution on top of the number density evolution at $z > 8$.

Thus it is important to get a clearer picture from the observational side before one can draw any firm conclusions on the nature of the star formation at $z \geq 6$. Nevertheless, the exercise presented here clearly suggests that strong constraints on the nature of star formation can be obtained once there is improvement in the observations. In particular accurately measured luminosity functions over small redshift intervals at $z > 6$ will provide important constraints on the nature of reionization. We expand on this point in the following section.

6 PROBING THE REIONIZATION HISTORY WITH $z \geq 6$ LUMINOSITY FUNCTION

We now investigate further the possibility of using the redshift evolution of the observed luminosity function to probe the reionization history of the universe. In particular we are interested in the effect of molecular cooled halos and star burst activity during dark ages. In our model calculations the luminosity function at the low luminosity end is mainly produced by low mass halos that are affected by radiative feedback. As discussed before, the radiative feedback results in a break in the luminosity function that corresponds to halos with circular velocity of 90 km s^{-1} for $z < z_{re}$. However, the exact luminosity at which this break will appear in the luminosity function depends on the amount (f_*) and duration ($\kappa\, t_{dyn}$) of star formation and the IMF (for example the value of $m_{\rm low}$). We illustrate to begin with, the effects of reionization feedback in a general manner, and then more specifically in relation to Richard et al. data.

In the left side panels of Fig. 14, we show the luminosity functions at different redshifts predicted by a set of self-consistent models with molecular cooled halos incorporating reionization feedback. The solid, dotted and short-dashed curves are for our models M_1, M_2, and M_3 respectively, (see Fig. 2 and Table 3). Note that the model M_1 and M_2 differ only in f_* for molecular cooled halos and both have atomic cooled halos as in model A. Model M_3 is same as M_2 but with $m_{\rm low} = 50$ M$_{\odot}$ in the molecular cooled halos. The redshifts of reionization in these models are 10.8 , 5.9 and 11.6 respectively (see Table. 3). It is clear from Fig. 14 that

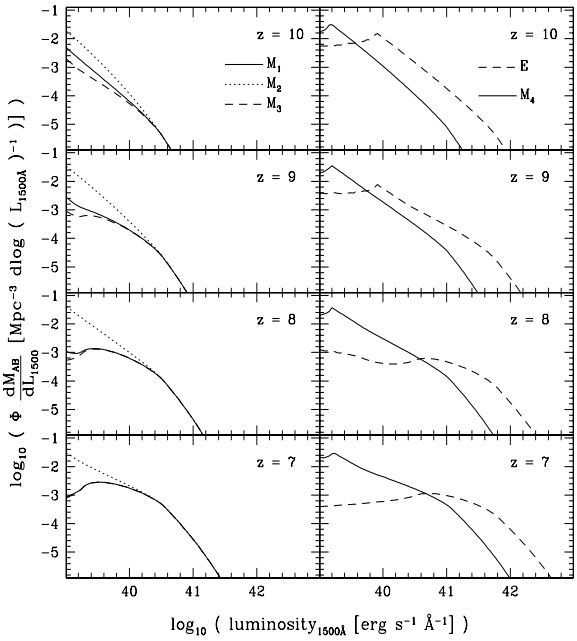

Figure 14. Luminosity functions for $z = 7,\ 8,\ 9$ and 10 are plotted from bottom to top. In the left side panels the solid, dotted and short-dashed curves are for our models M_1, M_2 and M_3 respectively (see Fig. 2 and Table 3 for reference). All these models assume $\eta = 4.5$. The solid and long-dashed curves in the right side panels are for model E with $\eta = 1$ and model M_4 with $\eta = 4.5$ respectively.

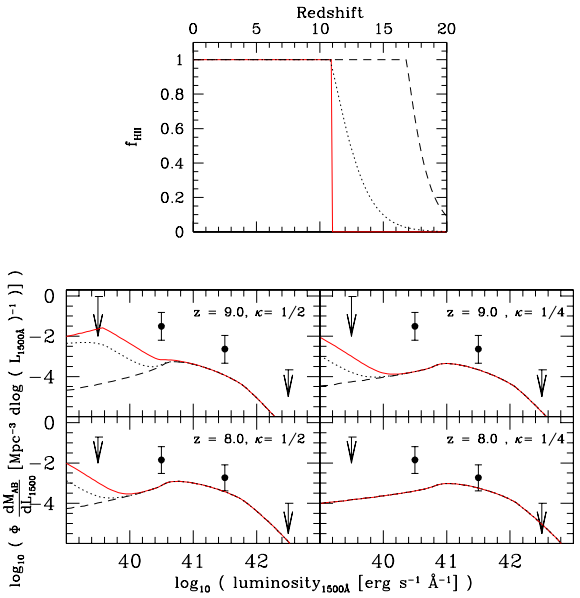

Figure 15. The effects of early reionization. Top panel shows three fiducial reionization scenarios. The dashed line is for $z_{re} = 16.8$ and $\tau_e = 0.236$, dotted line is for $z_{re} = 10.9$ and $\tau_e = 0.142$. The solid line assume an abrupt reionization at $z_{re} = 10.9$ which produces an optical depth of $\tau_e = 0.111$. Rest four panels show the luminosity functions obtained with these reionization models at different redshifts for our top heavy model ($10 - 100\ M_\odot$) with $f_* = 0.50$ and $\eta = 1.0$. Middle panels show the the luminosity function for $z = 9.0$ with $\kappa = 1/2$ (middle left panel) and $\kappa = 1/4$ (middle right panel). The bottom panels are for $z = 8.0$ with $\kappa = 1/2$ (bottom left panel) and $\kappa = 1/4$ (bottom right panel). We follow the same line style as top panel for different reionization models.

the luminosity function from these three models are identical at $L(1500) \gtrsim 10^{40.4}$ erg s^{-1}Å^{-1}. In the low luminosity end models M_1 and M_3 produces similar luminosity function but differ significantly from that of model M_2. This difference is due to the early suppression of low mass halos in models M_1 and M_3 due to early reionization. It is clear from this illustration that even though the molecular cooled halos are not directly detectable, their contribution to reionization can be probed using an accurately measured redshift evolution of luminosity function at $z \geq 6$.

In the right side panels of Fig. 14 we plot the results for model M_4 and E in solid and long-dashed lines respectively. In model M_4 we use $\kappa = 1/4$ and normal IMF in all the halos. Whereas in model E we use $\kappa = 1/9$ and top-heavy IMF. In these models star formation occurs over a short time scale, compared to the models where $\kappa = 1$. As expected, both the models therefore clearly produce a larger number of luminous galaxies at $L(1500) \geq 10^{41.4}$ erg s^{-1}Å^{-1}. These two models have similar optical depth to reionization, $\tau_e = 0.114$ for model E, and $\tau_e = 0.121$ for model M_4. However one can see from Fig. 14, that the slope of their luminosity functions, at the low luminosity end, are very different. The reason for this lies in the two models having different z_{re}. For model M_4, the redshift of reionization $z_{re} = 6.2$. As this is lower than the z range over which we study the luminosity function we do not see a significant flattening in the luminosity function at low luminosities. On the other hand, in the case of model E the reionization occurs at $z_{re} = 8.4$. The resulting sudden change in the luminosity function at $z \leq 8$ compared to that at high-z is clearly visible in Fig. 14. The break in the luminosity occurs around $L(1500) = 10^{41}$ erg s^{-1}Å^{-1}. This example clearly demonstrates that one can have detectable changes in the luminosity function close to z_{re}.

In summary, if the ionization feedback is the main contributor to the suppression of star formation activities in the low mass halos then the redshift of reionization can be constrained from the epoch at which the low luminosity flattening occurs in the galactic luminosity function. In the presence of star bursting activities or low dust extinction we expect the break luminosity to be occurring at $L(1500) \sim 10^{41}$ erg s^{-1}Å^{-1} that is easily detectable with the present day telescopes. Hence, we can use the low end of the luminosity function at high-z as an indicator to the reionization history whereas the high end of the luminosity function can probe the mode of star formation.

Now consider more specifically the constraints implied by the Richard et al. data. As explained in the previous section to reproduce the observations of Richard et al. (2006) we need a burst mode of star formation with no reddening correction for UV light. In all our self-consistent atomic cooled models reionization occurs at $z_{re} < 10$ (see Table 2). The effect of this is reflected in Figs. 8 and 9 where the predicted number density of galaxies with luminosity of order 10^{40} erg s^{-1}Å^{-1} is higher at $z \geq 8$ than that at $z < 8$ (whereas naively one would have expected it to be the other way round). Higher value of f_{esc} or the inclusion of molecular cooled halos would produce reionization at higher redshifts (see Table 3). We explore the effect of such early reionization to the predicted luminosity function for $z > 6$ in Fig. 15. In the top panel of Fig. 15, we present three fiducial reionization scenarios. The dashed line represents a very early reionization of $z_{re} = 16.8$ and the corresponding optical depth is $\tau_e = 0.236$. This scenario is considered, for illustrative purposes, in the view of 1st year WMAP data (Spergel et al., 2003), (where a $\tau_e = 0.17^{+0.08}_{-0.07}$ was

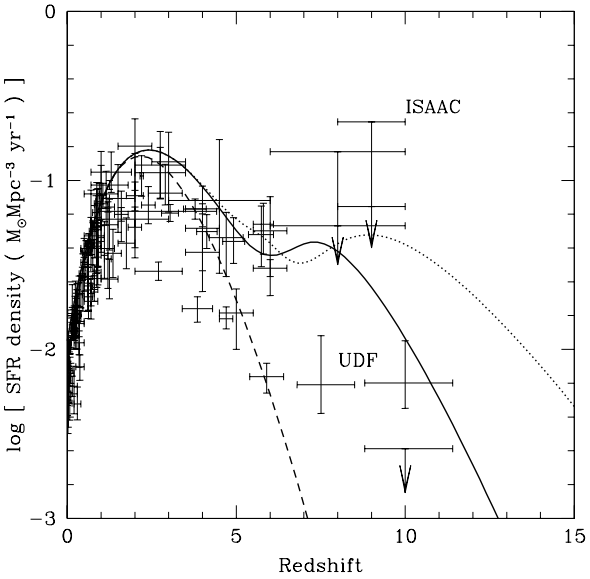

Figure 16. Redshift evolution of SFR density. The observed data points are a compendium of all the available observations obtained by Hopkins & Beacom (2006) and scaled down by a factor of 2.5 to make it consistent with the IMF used in our models. The solid and dotted lines are the total SFR density calculated from Eq. (4) for model A and M_2 respectively. The dashed line is the SFR density obtained by integrating the luminosity function up to $0.3L^*_{z=3}$ for model A.

favored). The dotted line represents a reionization model which has $z_{re} = 10.9$ and $\tau_e = 0.142$. In these two models the hydrogen ionization fraction changes in a continuous fashion. We have considered a third model (solid line) where reionization occurs abruptly at $z_{re} = 10.9$. This leads to an optical depth $\tau_e = 0.111$. This model mimics the reionization model taken by the WMAP team to get the reionization redshift from the electron optical depth using third year data (Spergel et al., 2006). The rest of the panels of Fig. 15 show the luminosity function obtained for above mentioned three reionization models. For the model with $z_{re} = 16.8$ (dashed curves) we see a clear turnover in the luminosity function at $L(1500) \sim 10^{41}$ erg s^{-1}Å^{-1} due to photoionization suppression. Clearly it will become more difficult to explain the luminosity function of Richard et al. (2006) especially for $L(1500) < 10^{41}$ erg s^{-1}Å^{-1}. It is more interesting to note the presence of low luminosity galaxies in the other two cases. In these cases the detected low luminosity galaxies are the ones that formed prior to reionization. Number of such galaxies are larger when one considers a higher value of κ (or prolonged star formation activities). The difference between the dotted and the dashed luminosity function arises mainly from the redshift dependence of f_{HII} prior to the reionization. Thus accurately measuring the luminosity function of galaxies at these epochs will give an independent constraint on the epoch and nature of reionization.

7 REDSHIFT EVOLUTION OF THE SFR DENSITY

Most of the semi-analytic models in the literature use the observed star formation rate density to fix model parameters. In this section we discuss the evolution of SFR density in detail in the frame work of models discussed here. The SFR density and its redshift evolution in our model is given by Eq. (4). However, observationally, one determines only the luminosity function above some luminosity threshold. The SFR density is then estimated by integrating the luminosity function and using continuous star formation with a set of IMFs. In Fig. 16 we show the observed SFR density obtained by Hopkins & Beacom (2006) from the compendium of all the available observations and our predictions for a few models. We have also added the results of Richard et al. (2006) and Bouwens et al. (2005) at $z \geq 6$ with a reddening correction of $\eta = 4.5$.

First we consider our fiducial model A. Recall that this model adopts a Salpeter IMF with $1 - 100\ M_\odot$. This leads to a UV luminosity a factor 2.5 larger than a Salpeter IMF with $0.1 - 100\ M_\odot$, canonically used to calculate the SFR density from the observed luminosity function. We have therefore scaled down the observed data points given by Hopkins & Beacom (2006) appropriately. The continuous curve in this figure is SFR density given by Eq. (4) for our model A. This curve fits the observed SFR density for $z \leq 6$ and has a second peak at $z \sim 7.5$ before declining with increasing redshift. Such a high redshift peak is predicted by semi-analytical models with photoionization feedback (see for example: Barkana & Loeb, 2001 and Choudhury & Srianand 2002). It has also been pointed out that the peak becomes more pronounced and moves towards high-z if one includes molecular cooled low mass halos in the calculations. This can be seen from the dotted curve in the figure which shows the result for model M_2. Thus if one considers only the global SFR density, it appears that the existence of the second peak at high-z could explain the Richard et al's point in this figure. However, as we have already mentioned the observed SFR density is obtained by integrating the luminosity function up to $0.3L^*_{z=3}$. In Fig. 16 we have also shown the SFR density calculated with this prescription (dashed line) for model A. The corresponding behavior for model M_2 is similar to this dashed curve. It is clear that with this prescription the SFR density is always less than that computed from Eq. (4). The difference become more and more as one moves towards the higher redshifts as the number of low mass halos increases with the increasing redshift. Clearly the second peak that is visible in the solid curve disappears when we use the low luminosity cutoff while computing the SFR density. Consistent with our discussions on the luminosity function, our models that fit $z < 6$ luminosity functions will not be able to explain SFR density obtained from the Richard et al's observations.

Therefore, even though semi-analytical models predict the SFR density in a simple analytic form, in order to compare with the observations it is important to model the luminosity function as we have done here. Since observations are not very sensitive to the star formation activities in the low mass halos the measurement of SFR density directly from the observations will grossly under predict the actual star formation rate density especially at high-z. In this regard redshift distribution GRBs will provide a very useful probe of the star formation rate density at $z \geq 6$, if they trace the underlying star formation rates (Barkana & Loeb, 2001; Choudhury & Srianand 2002).

8 DISCUSSIONS AND CONCLUSIONS

We have presented here a semi-analytic formalism for computing (i) star formation, (ii) reionization (iii) UV luminosity functions and (iv) source counts using a modified PS formalism, taking into account the cooling constraints, radiative feedback and suppression of star formation in high mass halos.

We find that even if star formation is hosted only in large atomic cooled halos the universe is sufficiently reionized to be con-

sistent with the $\tau_e = 0.09 \pm 0.03$ inferred by WMAP 3rd year data, for a range of star formation scenarios. Also the inferred reionization redshifts are consistent with observations of the highest redshift QSOs (Fan et al. 2006) and Lyman-α emitters (Iye et al. 2006). The inclusion of star formation in molecular cooled halos increases the value of τ_e. However, the recent WMAP observations are better consistent with a low efficiency of the molecular cooled halos in reionizing the universe.

The major focus of our work here is on a self-consistent modelling of the observed UV luminosity function of galaxies, its evolution at high redshifts and then using this to probe the nature and evolution of star formation at high-z. Our semi-analytic models with the best fit cosmological parameters derived from WMAP 3rd year data fit the observed galaxy luminosity functions in the redshift range $3 \leq z \leq 6$, for a reasonable range of model parameters. The feedback due to photoionization is sufficient to explain the $z = 6$ luminosity function. However we need additional feedback, possibly due to supernova that suppresses star formation activities in halos with $10^{10} \lesssim (M/M_{\odot}) \lesssim 10^{11}$, to explain the low luminosity end at $z = 3$. Also the observed evolution of luminosity functions from $z = 6$ to $z = 3$ can easily be explained with a modest change in $m_{\rm low}$ of the Salpeter IMF, or the amount of dust reddening as expected from galaxy evolution. We require roughly 50% of the baryonic mass to go through star formation over few dynamical time-scales. This is consistent with the median gas fraction of 50% and the corresponding stellar mass inferred from the high-z Lyman break galaxies (Erb et al. 2006). The lensing measurements of Mandelbaum et al (2006) constrain the mean conversion efficiency of baryons to stars to be about 20%, with considerable error in some of their determinations (see their Table 3 and Figure 4). Note that upto about 35% of the mass going into stars, is returned back to the ISM by supernovae, for the IMF as in our Model A. Therefore $f_* = 0.5$ which we have adopted is not greatly in excess of even the above mean value. It is possible to have a smaller fraction of the baryons in a halo going into stars, by lowering κ, or by adopting a higher σ_8 or n_s than the fiducial values favored by the WMAP 3rd year data. The first possibility is however disfavored by the observations of Eyles et al (2007), which constrain the age of stellar populations in high-z galaxies.

The models that fit the luminosity function for $z \leq 6$ are consistent with the upper limits on the luminosity functions for $z = 7$ obtained by Mannucci et al. (2007) and the integrated source counts obtained by Bouwens et al. (2005) for $8 \leq z \leq 12$. The observed decline in the luminosity function with increasing z is naturally produced by the decline in the halo number density coming from structure formation models without any additional dramatic changes in the mode of star formation. However, if the three candidate galaxies tentatively identified by Bouwens et al. (2005) become confirmed as high-z galaxies then we required additional changes in the mode of star formation. Moreover, the average luminosity function obtained by Richard et al. (2006) for $6 \leq z \leq 10$ can only be understood if star formation occurs in a burst mode with high efficiency, top-heavy IMF and very little or no reddening correction for the UV light. These models produce more number of galaxies than the three obtained by Bouwens et al (2005). The difference between the two sets of available observations at $z > 6$ is perhaps much larger than the expected cosmic variance. Thus a convergence from the observational front is needed before we can draw any interesting conclusions on the nature of the star formation activities at $z \geq 6$. An important constraint arises from the fact that the rest UV-optical spectral energy distribution of considerable fraction of $z \sim 6$ galaxies show a Balmer break. This suggests prolonged star formation activities with considerable mass contributed by low and intermediate mass stars, at least in these high redshift galaxies (Eyles et al. 2007).

The abundance of low luminosity galaxies is quite sensitive to the photoionization feedback, and hence to the reionization history. Using a range of self-consistent reionization models we show that such a feedback can lead to a flattening or break in the high-z galaxy luminosity function at low luminosities ($L(1500) \lesssim 10^{41}$ erg s^{-1}Å^{-1}). Accurately measured luminosity functions in the redshift range $6 \leq z \leq 10$ can therefore be used to place interesting constraints on the epoch of reionization and the nature of star formation activities in the dark ages.

We compare our model predictions of star formation rate density with the observations. The observed SFR density is obtained by integrating the luminosity function up to some low luminosity limit ($0.3L^*_{z=3}$). This approach clearly under predicts the actual global star formation rate density especially at higher redshifts. As molecular cooled halos are expected to be fainter than the typical detection limits achieved in the deep field images, the star formation history constructed directly from the observations will miss any peak in the SFR density mainly due to such halos. In that case other tracers of star formation activities like GRBs will be much more useful in detecting the enhanced star formation activities in such low mass halos.

We have used here the modified Press-Schecter formalism of Sasaki (1994), to calculate the formation rate and survival probability of dark matter halos. Note that simply taking the time derivative of the PS or some other mass function, does not give the formation rate of halo, but only the formation minus the destruction rate. It would be interesting to obtain the formation rate directly from N-body simulations and repeat our calculations of high-z galaxy luminosity functions. Metallicity of the gas is one of the factors which could decide the nature of the stellar IMF (cf. Schneider et al 2006). Very low metallicity could favor a top-heavy IMF, while as the metallicity increases one may transit to a more standard Salpeter IMF. However, the time-scale over which the the metal enriched gas mixes with primordial gas is still a subject of debate; Jimenez and Haiman (2006) in fact point to observational evidence for top-heavy "primordial" star formation even at $z \sim 3$. In our present models we have not explicitly included such metallicity feedback. Although the redshift evolution of $m_{\rm low}$ required to fit the luminosity function between $z = 3$ and $z = 10$ in our models, is perhaps an indication of such a feedback. Our model calculations also do not consider the influence of outflows in suppressing star formation. Such outflows are important in enriching the IGM at high-z. And they could also play a role in providing the additional feedback that we clearly need in the case of $z = 3$ luminosity functions. We hope to return to some of these issues in more detail in future work.

ACKNOWLEDGEMENTS

We thank Iwata Ikuru and Johan Richard for kindly providing the data on luminosity function used here at $z < 6$ and $z > 6$ respectively. We also thank Andrew Hopkins for kindly providing the data on SFR density and Jasjeet Bagla for discussions. We thank an anonymous referee for insightful comments. SS thanks CSIR for providing support for this work.

REFERENCES

Alvarez, M. A., Shapiro, P., Ahn, K. Iliev, I. T., 2006, ApJ, 644, L101

Barkana, R., Loeb, A. 2001, PhR, 349, 125
Benson, A. J., Lacey, C. G., Baugh, C M., Cole, S., Frenk, C. S., 2002, MNRAS, 333, 156
Best, P. N., Kaiser, C. R., Heckman, T. M., Kauffmann, G., 2006, MNRAS, 368, L67
Bromm, V., Loeb A., 2002, ApJ, 575, 111
Bouwens, R. J., Thompson, R. I., Illingworth, G. D., Franx, M., van Dokkum, P. G., Fan, X., Dickinson, M. E., Eisenstein, D. J., Rieke, M. J., 2004, ApJ, 616, L79
Bouwens, R. J., Illingworth, G. D., Thompson, R. I., Franx, M., 2005, ApJ, 624, L5
Bouwens R., Illingworth G., 2006, NewAR, 50, 152
Bower, R. G., Benson, A. J., Malbon, R., Helly, J. C., Frenk, C. S., Baugh, C. M., Cole, S., Lacey, C. G., 2006, MNRAS, 370, 645
Chiu W. A., Ostriker J. P., 2000, ApJ, 534, 507
Choudhury, T. R., Ferrara, A., 2006, MNRAS, 371, L55
Choudhury, T. R., Srianand, R., 2002, MNRAS, 336, L27
Cowie, L. L., Songaila, A., Hu, E. M., Cohen, J. G., 1996, AJ, 112, 839
Croton et al, 2006, MNRAS, 365, 11
Dijkstra, M., Haiman, Z., Rees, M., Weinberg, D. H., 2004, ApJ, 601, 666
Eke V. R., Cole S., Frenk C. S., 1996, MNRAS, 282, 263
Eyles, L. P., Bunker, Andrew J., Ellis, R., Lacy, M., Stanway, E., Stark, D., Chiu, K., 2007, MNRAS, 374, 910
Erb, D. K., Shapley, A. E., Pettini, M., Steidel,C. C., Reddy, N. A., Adelberger, K. L., 2006, ApJ, 644, 813
Fan, X., Strauss, M. A., Richards, G. T. et al., 2006, AJ, 131, 1203
Greif, T. H., Bromm V., 2006, MNRAS, 373, 128
Gunn J. E., Peterson B. A., 1965, ApJ, 142, 1633
Haiman Z., Abel T., Rees M. J., 2000, ApJ, 534, 11
Haiman, Z., Bryan, ., 2006, ApJ, 650, 7
Hopkins, A., Beacom, J., 2006, ApJ, 651, 142
Hu, E., Cowie, L., 2006, Nature, 440, 1145
Iwata, I., Ohta, K., Tamura, N., Ando, M., Wada, S., Watanabe, C., Akiyama, M., Aoki, K., 2003, PASJ, 55, 415
Iwata, I., Ohta, K., Tamura, N., Akiyama, M., Aoki, K., Ando, M., Kiuchi, G., Sawicki, M., 2007, MNRAS (in Press)
Iye, M., et al., 2006, Nature, 443, 186
Jimenez, R., Haiman, Z., 2006, Nature, 440, 501
Juneau, S. et al., 2005, ApJ, 619, 135
Labbe, I., Bouwens, R., Illingworth, G. D., Franx, M., 2006, ApJ, 649, L67
Leitherer. C., et al., 1999, ApJS, 123, 3
Mandelbaum, R., Seljak, U., Kauffmann, G., Hirata, C. M., Brinkmann, J., 2006, MNRAS, 368, 715
Mannucci, F., Buttery, H., Maiolino, R., Marconi, A., Pozzetti, L., 2007, A&A, 461, 423
Nagamine, K., Ostriker, J. P., Fukugita, M., Cen, R., 2006, ApJ, 653, 881
Oke, J. B. and Gunn, J. E., 1983, ApJ, 266, 713
Padmanabhan T, Theoretical Astrophysics, 2002, Volume III, Cambridge University Press
Peebles P. J. E., Principles of Physical Cosmology, 1993, Princeton University Press, Princeton, New Jersey
Pettini, M., Shapley, A. E., Steidel, C., Cuby, J, Dickinson, M, Moorwood, A. F. M., Adelberger, K. L., Giavalisco, M., 2001, ApJ, 554, 981
Press W. H., Schechter P., 1974, ApJ, 187, 425
Reddy, N. A., Steidel, C. C., Fadda, D., Yan, L., Pettini, M., Shapley, A. E., Erb, D. K., Adelberger, K. L., 2006, ApJ, 644, 792
Richard, J., Pello, R., Schaerer, D., Le Borgne, J.-F., Kneib, J.-P., 2006, A&A, 456, 861
Sasaki S., 1994, PASJ, 46, 427
Sawacki M., Thompson D., 2006, AJ, 642, 653
Schaerer, D., 2003, A&A, 397, 527
Schneider R., Salvaterra R., Ferrara A, Ciardi B., 2006, MNRAS, 369, 825
Somerville, R. S., Primack, J. R., 1999, MNRAS, 310, 1087
Spergel D. N. et al., 2003, ApJS, 148, 175
Spergel D. N. et al., 2006, ApJ (in Press)
Springel, V., Hernquist, L., 2003, MNRAS, 339, 289
Steidel, C. C., Adelberger, K. L., Shapley, A. E., Pettini, M., Dickinson, M., Giavalisco, M., 2003, ApJ, 592, 728
Tegmark M., Silk J., Rees M. J., Blanchard A., Abel T., Palla F., 1997, ApJ, 474, 1
Thoul A. A., Weinberg D. H., 1996, ApJ, 465, 608
Wyithe, J. S. B., Loeb, A., Carilli, C., 2005, ApJ, 628, 575